Palaeogeography, Palaeoclimatology, Palaeoecology 510 (2018) 109–123

Contents lists available at ScienceDirect

Palaeogeography, Palaeoclimatology, Palaeoecology

journal homepage: www.elsevier.com/locate/palaeo

Rock magnetic record of late Neogene red clay sediments from the Chinese Loess Plateau and its implications for East Asian monsoon evolution

Yougui Song[a,*], Xiaomin Fang[b], Xiuling Chen[c], Masayuki Torii[d], Naoto Ishikawa[e], Maosheng Zhang[f], Shengli Yang[g], Hong Chang[a]

[a] State Key Laboratory of Loess and Quaternary Geology, Institute of Earth Environment, Chinese Academy of Sciences, Xi'an 710061, China
[b] Key Laboratory of Continental Collision and Plateau Uplift, Institute of Tibetan Plateau Research, Chinese Academy of Sciences, Beijing 100101, China
[c] Institute of Geography, College of Geographical Sciences, Fujian Normal University, Fuzhou 350007, China
[d] Faculty of Informatics, Okayama University of Science, Okayama 700-0005, Japan
[e] Graduate School of Human and Environmental Studies, Kyoto University, Kyoto 606-8501, Japan
[f] Key Laboratory for Geo-hazard in Loess Area, Xi'an Centre of Geological Survey, Ministry of Land and Resources of China, Xi'an 710054, China
[g] Key Laboratory of Western China's Environmental Systems, College of Earth and Environmental Science, Lanzhou University, Lanzhou 730000, China

ARTICLE INFO

Keywords:
Late Miocene
Pliocene
Global cooling
Tectonic events
Magnetic minerals

ABSTRACT

The Quaternary loess–paleosol and underlying Neogene red clay sequences on the Chinese Loess Plateau (CLP) contain a remarkable continental record of past East Asian monsoon changes and aridification of the Asian interior. While monsoon variability during the Quaternary is reasonably well understood, the evolution and dynamics of the monsoon during the Neogene are still debated. The rock magnetism of aeolian sediments is a well-established tool for reconstructing the palaeoclimatic history of Asia. Here, we present a rock magnetic record from Late Neogene red clay sediments of the Chaona section in the central CLP. The results indicate that the main magnetic minerals in the red clay are magnetite, maghemite, hematite and goethite, similar to the overlying Quaternary loess-palaeosol sequences. The high-resolution rock magnetic record, combined with the results of other proxies, demonstrate a stepwise intensification of the summer monsoon and a progressive enhancement of the winter monsoon in East Asia during the Late Neogene. Based on the results, the climatic evolution of East Asia can be divided into three intervals: Interval III, from 8.1 to 6.8 Ma, is characterized by a cool, dry climate with a relatively weak East Asian Summer Monsoon (EASM) and East Asian Winter Monsoon (EAWM); Interval II, from 6.8 to 4.3 Ma, is characterized by cool/warm cycles; and Interval I, from 4.3 to 2.8/2.6 Ma, was warm and humid, and within which the EASM strengthened rapidly and the EAWM fluctuated considerably, with an increasing trend. We infer that before 4.3 Ma the variations of both the EASM and EAWM were closely related to global cooling and that the intensified EASM during the late Pliocene was primarily caused by tectonic events, including the gradual closure of the Panama Seaway and the uplift of the Tibetan Plateau, rather than by global cooling.

1. Introduction

The Quaternary loess-paleosol sequences of the Chinese Loess Plateau (CLP) have been systematically investigated (An et al., 1990; Guo et al., 1996; Heller and Liu, 1982; Kukla et al., 1988; Liu, 1985; Lu and An, 1998; Sun et al., 2012) and are regarded as some of the most complete terrestrial records of Quaternary climatic change. During the last two decades, the Neogene red clay (or red earth) underlying the Quaternary loess has also been widely investigated. It is also of aeolian origin (Guo et al., 2001) and accumulated during the Late Miocene, mainly from 8–7 Ma, in the central and eastern CLP (Ao et al., 2016; Ding et al., 1998; Qiang et al., 2001; Song et al., 2001b; Sun et al., 1998b; Xu et al., 2009), and in the Late Oligocene to Early Miocene, at 25–22 Ma (Guo et al., 2002; Hao and Guo, 2007; Qiang et al., 2011), in the western CLP. The thick and continuous red clay sequences provide a wealth of information about Miocene-Pliocene East Asian Monsoon (EAM) evolution and the aridification of the Asian interior (An, 2000; An et al., 2001; An et al., 1990; Guo et al., 2002; Qiang et al., 2011), and they are arguably one of the few continuous terrestrial archives available for studying the forcing mechanisms of Pliocene climate (Ao et al., 2016; Ding et al., 2000; Lu and Guo, 2014; Nie et al., 2014a; Sun et al., 2010).

* Corresponding author.
E-mail address: ygsong@loess.llqg.ac.cn (Y. Song).

http://dx.doi.org/10.1016/j.palaeo.2017.09.025
Received 25 July 2017; Received in revised form 20 September 2017; Accepted 21 September 2017
Available online 23 September 2017
0031-0182/

Previous studies of the aeolian deposits in northern China have extended the EAM history back to the late Oligocene (Qiang et al., 2011; Sun and Wang, 2005) or Early Miocene (Guo et al., 2002). Numerous sedimentological, geochemical, and paleontological studies, mainly from the CLP and in the South China Sea (SCS), have contributed significantly to our understanding of the changes in the EAM during the late Cenozoic. However, the record of Miocene-Pliocene evolution of the EAM preserved in the Neogene red clay sequence is still not well understood (Ao et al., 2016; Nie et al., 2015; Sun et al., 1998b; Vandenberghe et al., 2004; Zhang et al., 2007), which hinders our understanding of the driving mechanisms of the EAM. The relative intensities of monsoonal winds, precipitation and temperature, and their interrelationship (F. Li et al., 2014a; Nie et al., 2016; Nie et al., 2013), remain poorly constrained. Records from different climate proxies are inconsistent and in some cases the interpretations are contradictory. For example, the grain size (Sun et al., 2006; Vandenberghe et al., 2004), sedimentation rate (Sun and An, 2002), and pollen assemblages (Miao et al., 2011; Sun and Wang, 2005; Wu et al., 2007) of Neogene sediments indicate a strong winter monsoon and pronounced aridification of the Asian interior (Guo et al., 2002, 2004; Sun and An, 2002) since the Miocene. However, $^{87}Sr/^{86}Sr$ ratios (Wang et al., 2007) and Zr/Rb ratios (Chen et al., 2006) from the Lingtai red clay sequence imply that the East Asian Winter Monsoon (EAWM) strength was weak and relatively stable during the late Neogene. Red clay records from the CLP indicate that the East Asian Summer Monsoon (EASM) strengthened in stepwise fashion since the late Miocene (An, 2000; An et al., 2001; Sun et al., 1998a, 1998b). A stepwise intensification since 8.5 Ma was recorded by mineralogical records from ODP Site 1143 in the southern SCS (Wan et al., 2006); however, planktonic foraminiferal Mg/Ca and $\delta^{18}O$ records from ODP Site 1146 in the northern SCS indicated that the EASM weakened after 7.5 Ma (Steinke et al., 2010). Thus it is clear that more work is needed to clarify the nature of the evolution of the EAM.

Rock magnetic proxies have been widely used to reconstruct the history of the EAM (An et al., 1991; Evans and Heller, 2001; Heller and Liu, 1984; Liu et al., 2007; Maher, 2016; Nie et al., 2007). In addition, numerous magnetic studies have been undertaken on the Quaternary loess-paleosol sequences (An et al., 1991; Bloemendal et al., 1995; Deng et al., 2004; Evans and Heller, 2001; Heller and Liu, 1984; Maher, 2016; Y.G. Song et al., 2014b). In contrast, much less rock magnetic work has been undertaken on the red-clay sequence of the CLP (Liu et al., 2003; Nie et al., 2010b, 2013, 2016; Qiang et al., 2005; Song et al., 2007). Although field observations suggest that the degree of pedogenesis of the Neogene red clay is much stronger than that of the overlying Quaternary paleosols, the magnetic susceptibility records of all of the red clay sections from the central CLP exhibit overall lower values and long-term cyclic changes (An, 2000; An et al., 2001; Ao et al., 2016; Ding et al., 1998; Song et al., 2007; Sun et al., 1998a). Therefore, deciphering the climatic significance of the magnetic properties of the red clay is important for reconstructing paleoclimatic and paleoenvironmental changes in the region. Here we present the results of a systematic rock magnetic study of a red clay section in the central CLP and use the results to provide evidence for EAM changes during the late Miocene and Pliocene.

2. General setting and sampling

The Chinese Loess Plateau (CLP) covers some 640,000 km^2 in northern China and the climate of the region is mainly controlled by the seasonal alternation of the East Asian summer and winter monsoons. Geomorphologically, the CLP is divided into western and eastern/central parts by the NW-SE-oriented Liupan Mountains (Mts.) (Fig. 1). To the west of the Liupan Mts. is the Longzhong Basin which forms the base of the western CLP and is tectonically a part of the Northeastern Tibetan Plateau (Song et al., 2005). The Longzhong Basin, which was tectonically active during the Cenozoic, is characterized by very thick (> 3000 m), ancient (up to Paleocene), strongly folded and mainly fluvial-lacustrine and alluvial sediments, including the Paleogene Guyuan Group and the Neogene Gansu Group (Alonso-Zarza et al., 2009; Dupont-Nivet et al., 2007; Fang et al., 2015; Li et al., 2006; Yue et al., 2001), and aeolian red clay/earth sediments with an age of 25–22 Ma (Guo et al., 2002; Hao and Guo, 2007; Qiang et al., 2011). In contrast, the oldest aeolian red clay in the central/eastern CLP only extends to the late Miocene, about 8–7 Ma (Ding et al., 1998; Qiang et al., 2001; Song et al., 2001b; Sun et al., 1998b; Zhu et al., 2008), or 11–8 Ma in the eastern CLP (Ao et al., 2016; Xu et al., 2009). These age differences can be attributed to the uplift of the Liupan Mts. and the disaggregation of the Ordos plantation surface during the late Miocene resulting from the growth of the Northeastern Tibetan Plateau (Li et al., 2013; Song et al., 2001a, 2005; Yue et al., 2007). The broken and undulating landform was favorable for accumulating aeolian sediments.

The Chaona loess-red clay sequence (35°06′N, 107°12′E) in the central CLP (Fig. 1) provides a continuous paleoenvironmental record for the late Cenozoic. The red clay sequence is composed of two natural outcrops with about 20 m of overlap. Magnetostratigraphic studies indicate that the red clay was deposited from 8.1 to 2.6 Ma (Song et al., 2007) (Fig. 2). The 125-m-thick sequence of late Neogene red clay rests unconformably on lower Cretaceous sandstone and is overlain by a ~175-m-thick continuous Quaternary loess-palaeosol sequence. The red clay sequence is subdivided into five lithologic units, which are described in detail in Song et al. (2007). During the past decade, the pollen (Ma et al., 2005; Wu et al., 2007), carbonate (Chen et al., 2007), and heavy mineral (Nie and Peng, 2014; Nie et al., 2014a; Peng et al., 2016) content, together with the magnetic susceptibility enhancement mechanism (Nie et al., 2007, 2010a; Zhang et al., 2016), and their palaeoenvironmental significance (Nie et al., 2010b, 2013, 2014c), have been investigated. However, the various proxies exhibit different overall trends and patterns of variability (Fig. 2). For example, although the magnetic susceptibility (χ) record exhibits a long-term increasing trend until 2.6 Ma, the grain-size proxies (clay content and mean grain-size) remain relatively uniform but with high-frequency oscillations superimposed, with an abrupt change at ~3.3 Ma. This clearly contrasts with the strongly coupled relationship between these proxies in the Quaternary loess-paleosol sequences. The variation of the color parameter a* (redness) is also inconsistent with the stratigraphy; e.g., the reddest red clay sediments observed in the field have relatively low a* values. The rock magnetic properties are to some extent related to the bulk sediment grain size and bulk mineralogy, especially the content of iron-bearing minerals.

An astronomically-tuned high-resolution time series has been established for the sequence (Han et al., 2011) based on magnetostratigraphy and a grain-size record (Lü et al., 2001). This previous work provided us with a reliable chronological framework within which to conduct a detailed rock magnetic study. We selected about 705 bulk samples from the red clay sequence, at intervals of 10–20 cm, for hysteresis loop and other magnetic measurements, to reconstruct East Asia paleoclimatic and paleoenvironmental changes and to determine the potential climatic driving mechanisms.

3. Methods

About 300–500 mg of powdered sample was used for measurement of temperature-dependent magnetic susceptibility (χ–T curves) using an Agico KLY3 Kappabridge equipped with a CS3 high-temperature furnace. The measurements were made from room temperature to 700 °C and back to room temperature. An empty furnace tube was measured to determine the temperature-dependent background before measuring the sediment samples, and the susceptibility of each sample was obtained by subtracting the measured background value. The χ–T experiments were carried out at the Paleomagnetic Laboratory at Fort Hoofddijk, Utrecht University. In addition, the variation of the magnetization with temperature (M_s–T curves) was measured in air using a horizontally-balanced magnetic balance (EIKO system) at Kyoto

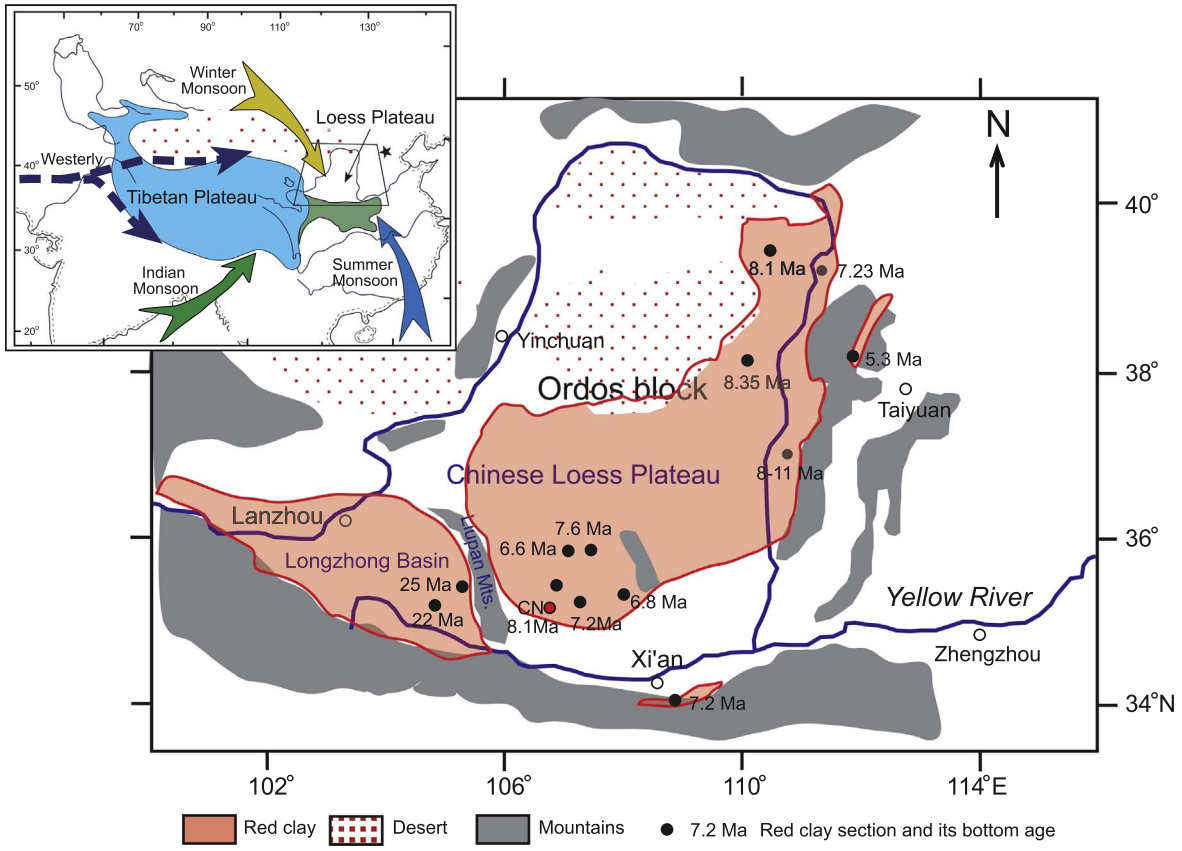

Fig. 1. Location and basal ages of various red clay sections (black circles) on the Chinese Loess Plateau. The red circle indicates the location of the Chaona section (this study). Inset map shows the location of the study region in Asia and the trajectories of the monsoonal circulation systems. (For interpretation of the references to color in this figure legend, the reader is referred to the web version of this article.)

University. The measurements were made from room temperature to 700 °C, with an inducing field of 0.85 T and a heating rate of 8 °C/min.

Isothermal remanent magnetization (IRM) acquisition curves were determined using a 2G pulse magnetizer (Model 660) with increasing fields applied to a maximum of 1.8 T; 17 field steps were used. In addition, thermal demagnetization of a three-component IRM was used to distinguish between magnetic minerals with different coercivities based on their individual unblocking temperature (Lowrie, 1990). Composite IRMs were imparted parallel to the three orthogonal axes of each sample, with fields of 2.7, 0.5 and 0.1 T, corresponding to hard, intermediate and soft magnetic components, respectively. The samples were then subjected to stepwise thermal demagnetization to reveal the unblocking temperature spectra for the three coercivity ranges. The remanences were measured with a 2G cryogenic magnetometer (Model 760) at Kyoto University.

Magnetic hysteresis parameters were measured using an Alternating Gradient Magnetometer (AGM) Micromag™ 2900 model at the paleomagnetism laboratory of Kyoto University, with a maximum field of 1.0 T and a 2 mT increment. Saturation magnetization (M_s), saturation remanent magnetization (M_{rs}) and coercive force (B_c) were calculated after removal of the paramagnetic component. Remanent coercivity (B_{cr}) was measured by applying a forward field of 1.0 T followed by the application of reverse fields of increasing strength and the change in remanence measured at each step. The results enable various interparametric ratios to be calculated using the IRM imparted at a high field (here 1.0 T) and the back IRM value at various reverse field strengths (e.g. −0.3 T). These parameters reflect variations in the coercivity spectrum of the magnetic mineral assemblage and therefore the mineralogy and grain size. A frequently used parameter, S-ratio, was calculated as S-ratio = $[(-\mathrm{IRM}_{-0.3T}/\mathrm{SIRM}) + 1] / 2$.

4. Results

4.1. Temperature-dependence of magnetization and magnetic susceptibility

M_s–T and χ–T curves are frequently used to determine the magnetic mineralogy of samples based on the occurrence of critical temperature-dependent magnetic transitions, such as the Curie temperature, and the shape of the curves. Examples of the use of M_s–T curves to identify different magnetic minerals are given in Dunlop and Özdemir (1997), Evans and Heller (2001) and Thompson and Oldfield (1986). Compared with M_s–T curves, χ–T curves are especially sensitive to subtle changes in both the magnetic minerals and their grain-size distribution during heating/cooling cycles (Deng et al., 2004; Liu et al., 2005; Mullender et al., 1993; VanVelzen and Dekkers, 1999; Zan et al., 2017).

The M_s–T curves of all the samples exhibit irreversible behavior during heating and cooling with a significant magnetization loss always occurring between heating and cooling (Fig. 3). The magnetization of the heating curves decreased rapidly until around 580 °C, the Curie temperature of magnetite. Similar behavior is also observed in the χ–T curves (Fig. 4). Thus, magnetite is regarded as the predominant magnetization carrier. The changes in magnetization and susceptibility beyond 600 °C are too subtle to be able to detect the presence of hematite, either originally present or created during heating. The magnetization loss between heating and cooling may be attributed to the conversion of magnetite, partially oxidized magnetite, or thermally unstable maghemite, into weakly magnetic hematite during heating (Dunlop and Özdemir, 1997; Zhu et al., 1996). However, the gradient of the heating curves between 300 and 450 °C changes only slightly (Fig. 3), which argues against the presence of a significant amount of maghemite. There is some tendency for the loss of magnetization during heating to decrease with decreasing depth through the section, which

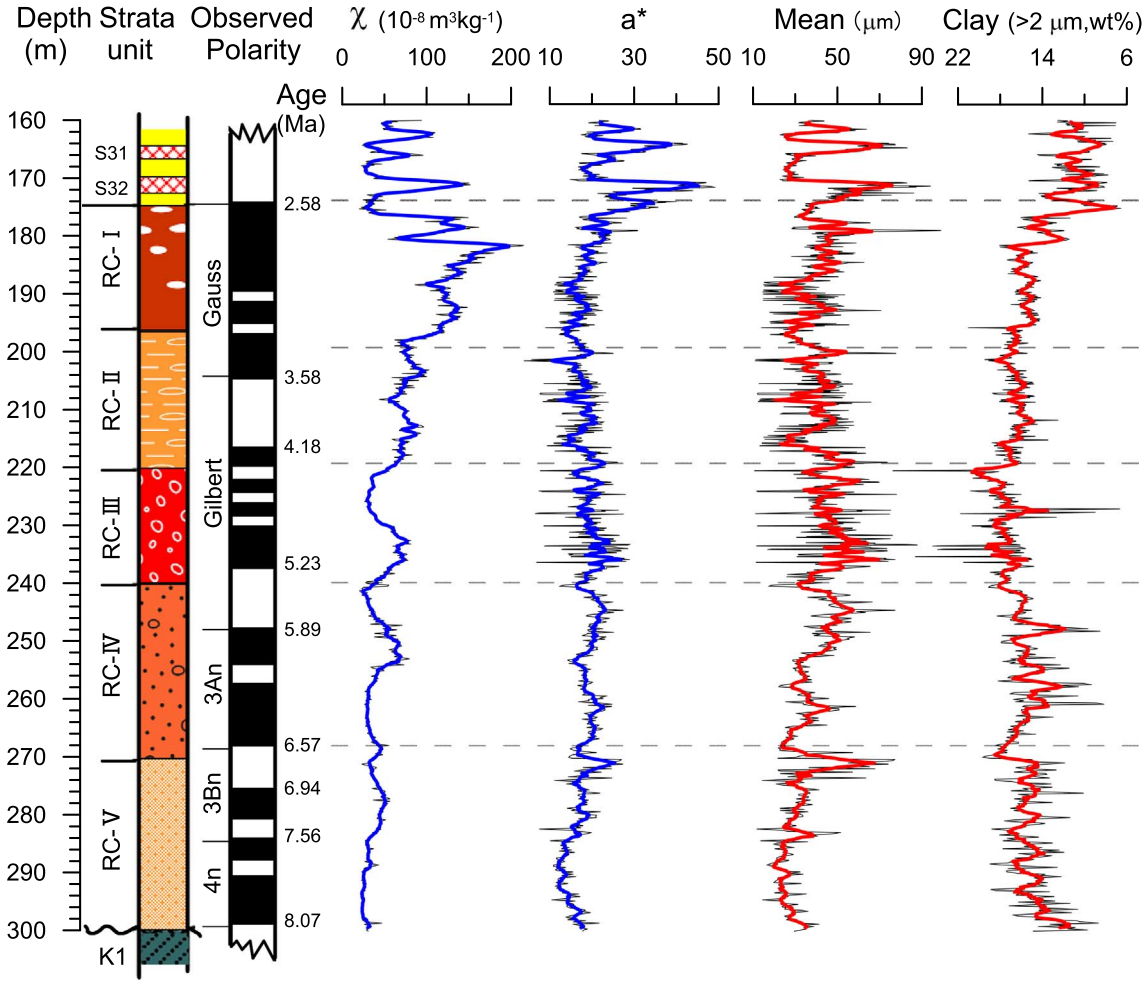

Fig. 2. Stratigraphy, paleomagnetic polarity (Song et al., 2007), magnetic susceptibility (χ) (Song et al., 2007), redness (a*) and grain size (mean grain-size and percentage clay content) (Lü et al., 2001) of the Chaona red clay section. (Bold curves are 7-point running averages). (For interpretation of the references to color in this figure legend, the reader is referred to the web version of this article.)

may indicate an increase in oxidized magnetite or maghemite since the late Miocene. This irreversible behavior is also observed in loess samples, in contrast to paleosol samples (Zan et al., 2017).

In contrast to the M_s–T curves, changes in the χ–T curves during heating and cooling are not obvious (< 10%), although sample CN1300 is an exception (Fig. 4). In all cases, χ increases gradually from room temperature to 200–250 °C, which may be caused by the gradual unblocking of fine-grained ferromagnetic particles. In addition, there is a small decrease in χ between ~200 °C and 400 °C, which may result from the conversion of metastable fine-grained maghemite to weakly-magnetic hematite (Liu et al., 2005). Finally, most of the samples exhibit a major decrease in χ at about 580 °C, which is consistent with the Curie temperature of magnetite. In the case of samples CN 9800 and CN 12420, χ continues to decrease to 680 °C without an evident inflection at 580 °C. The heating curves of samples CN4750 and CN11080 also continue to decrease between 580 °C and 680 °C, suggesting a relatively high concentration of hematite. On the other hand, the cooling χ–T curves rise rapidly from 600 °C to 400 °C, but there are only slight differences between the cooling curves and heating curves below 400 °C.

4.2. IRM acquisition curves

IRM acquisition analyses provide information about the coercivity distribution of samples which may be related to the grain-size characteristics and the mineralogy. The magnetization of hematite requires a much higher saturating field than does magnetite; the latter is typically saturated by 300–500 mT (Lowrie, 1990; Torii et al., 1996). The IRM acquisition curves of all the samples rise steeply at first, and reach over 90% saturation at 300 mT, indicating that the major proportion of the IRM is carried by low coercivity magnetic minerals such as magnetite and maghemite (Fig. 5). However, in most of the samples the IRM continues to rise gradually above 300 mT and is not completely saturated at the maximum field used (1.7 T), indicating the presence of high coercivity minerals such as hematite and goethite.

The thermal demagnetization curves of a three-component IRM reveal distinctive unblocking temperatures (Fig. 6). There is an obvious decrease in the IRM of the hard component (2.7 T) at 80 °C (sample CN760) or 120 °C (samples CN1750, CN6500, CN12200), indicating the presence of a significant goethite component. In addition, in most cases there is a monotonic decrease in the hard component from 80/120 °C to 680 °C, indicating the presence of hematite. The soft component (0.1 T) is completely demagnetized by around 580 °C, indicating the unblocking of magnetite. In the case of sample CN12200 there is an obvious change in the soft and intermediate components between 250 °C and 450 °C, suggesting the presence of maghemite or titanomaghemite (Lowrie, 1990). In terms of the absolute values of the three components, the soft components (magnetite and maghemite) are predominant, especially in the samples from the upper part of the section (CN760 and CN1750). In contrast, the hard components (hematite and goethite) are more significant in the samples from the lower part of the section (CN10200 and CN12200).

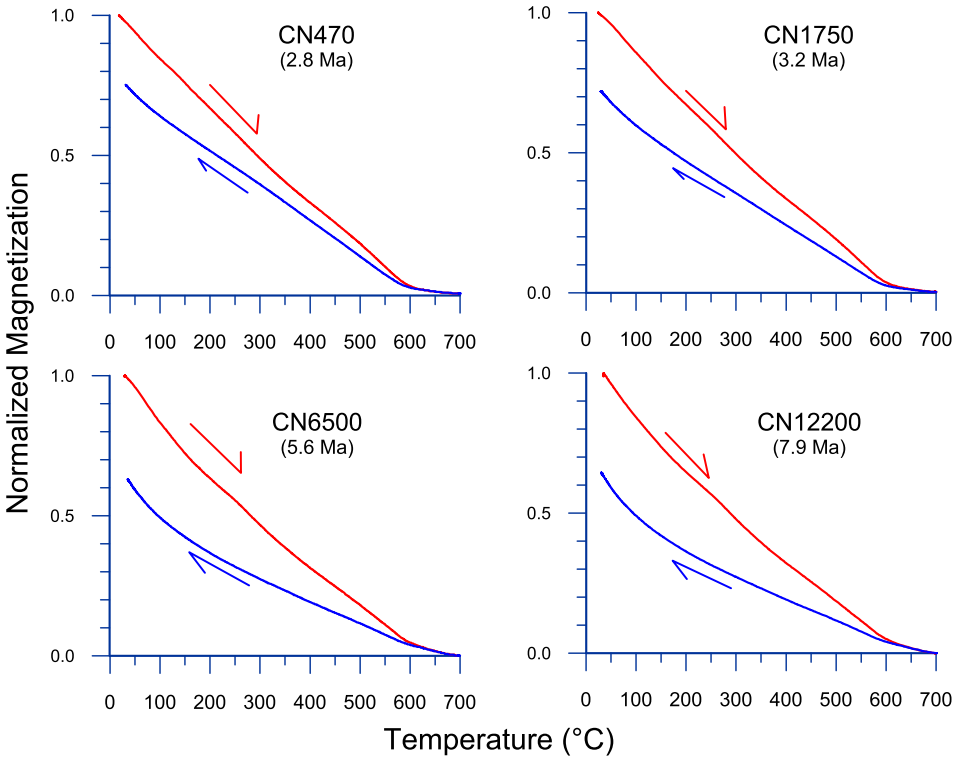

Fig. 3. Temperature dependence of magnetization (M_s–T curves) of red clay samples from the Chaona section in the Chinese Loess Plateau. Red (blue) curves indicate heating (cooling). (For interpretation of the references to color in this figure legend, the reader is referred to the web version of this article.)

4.3. Hysteresis properties

The shape of hysteresis loops can provide information about magnetic mineralogy, grain size and concentration, as well as the presence of paramagnetic minerals (Dunlop and Özdemir, 1997; Liu et al., 2007; Thompson and Oldfield, 1986). Loop width varies with the ratio of ferrimagnetic to antiferromagnetic minerals; the loop is broader if the ratio is low (Fukuma and Torii, 1998). The hysteresis properties of selected samples from the Chaona section are shown in Fig. 7. All the loops are 'S'-shaped, and they are, in general, similar to those of the overlying Quaternary loess and paleosols (Y.G. Song et al., 2014b). Samples with a higher susceptibility have narrower loops, especially in the case of those from the upper part of the red clay section (e.g., CN470, CN1080, CN1720, CN2720), and they tend to close at

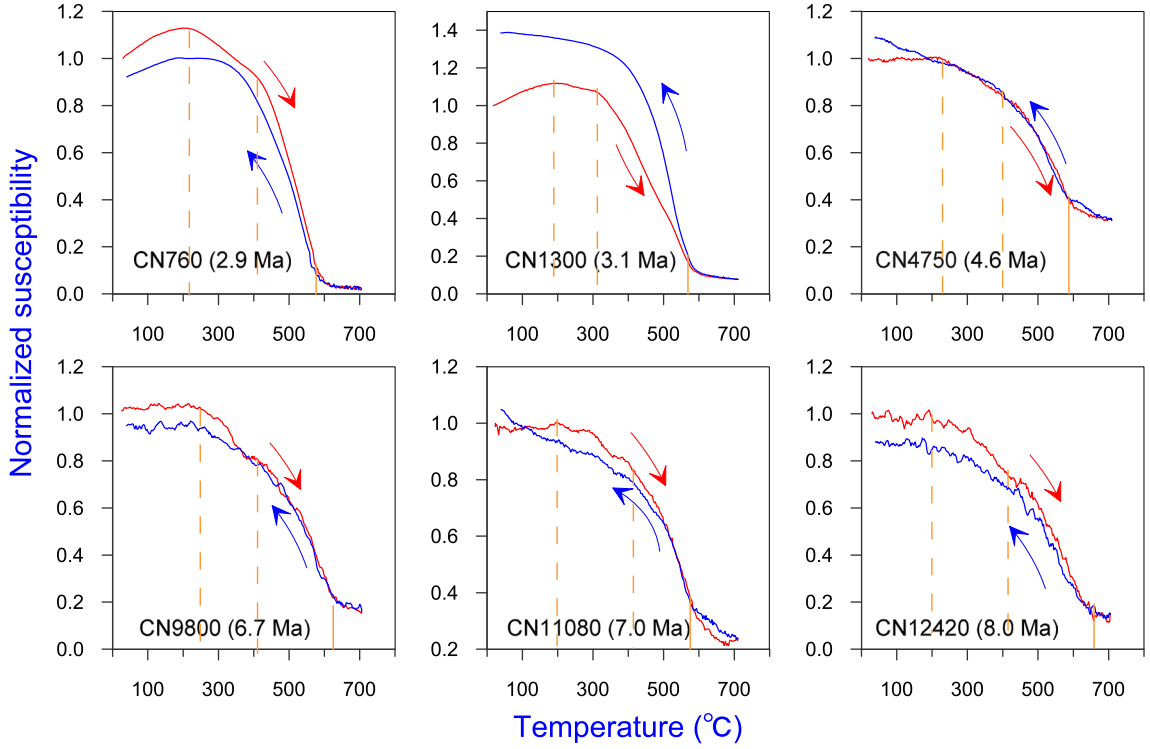

Fig. 4. Temperature dependence of magnetic susceptibility (χ–T) curves of representative red clay samples from the Chaona section. Red (blue) curves are heating (cooling) cycles. (For interpretation of the references to color in this figure legend, the reader is referred to the web version of this article.)

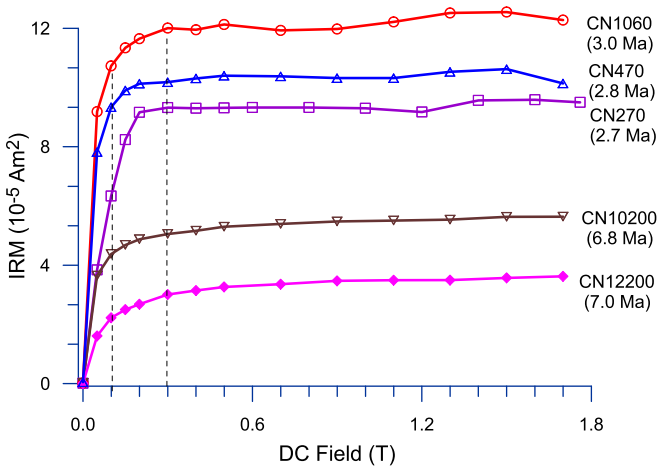

Fig. 5. IRM acquisition curves for the red clay samples from the Chaona section. The dashed vertical lines at 0.3 T are shown to differentiate between low- and high-coercivity portions of the curves.

100–200 mT; in addition, any constriction of the loop is largely suppressed. The higher M_s and M_{rs} values, and lower B_c and B_{cr} values, of these samples indicate that the magnetic properties are dominated by ferrimagnetic (soft) magnetic minerals such as magnetite and maghemite. The samples from the lower part of the section (e.g., CN8720, CN10280, CN11060, CN12140, CN12360), with lower susceptibility values, have typical wasp-waisted loops which are unclosed at 400 mT even 500 mT (Fig. 7). These samples have lower M_s and M_{rs}, and higher B_c and B_{cr} values, indicating the significant presence of imperfect antiferromagnetic (hard) magnetic minerals such as hematite and possibly goethite (Fukuma and Torii, 1998).

To obtain more information about the magnetic grain size of the red clay sediments, the B_{cr}/B_c and M_{rs}/M_s ratios were plotted on a Day plot which is widely used to diagnose the domain state (Day et al., 1977; Thompson and Oldfield, 1986). The results (Fig. 8) indicate that almost all the red clay samples fall within the pseudo-single domain (PSD) region, similar to the values of the loess and paleosol samples from the same section (Y.G. Song et al., 2014b) which are shown for comparison.

4.4. Temporal variation of rock magnetic parameters

Time series of rock magnetic parameters and selected inter-parametric ratios are shown in Fig. 9. Higher magnetic susceptibility (χ), M_{rs} and M_s values reflect higher concentrations of ferrimagnetic minerals such as magnetite and maghemite, while in contrast higher B_c and B_{cr} values reflect higher concentrations of antiferromagnetic minerals such as hematite and goethite (Dunlop and Özdemir, 1997; Fukuma and Torii, 1998; King and Channell, 1990; Thompson and Oldfield, 1986). In the Chaona red clay section there is a generally increasing trend in magnetic susceptibility, M_{rs}, M_s and S-ratio from 8.1 to 2.6 Ma, while B_c and B_{cr} fluctuate sharply with a slightly decreasing trend. The curves indicate frequent oscillations in magnetic mineral composition and concentration. The records can be divided into three intervals with boundaries of 6.8 Ma and 4.3 Ma; the three intervals roughly correspond to stratigraphic units RC-V, RC-IV and III, and RC-II and RC-I, respectively (Fig. 9).

In addition to the above, the following observations are noteworthy (Fig. 9): (i) The M_{rs} and M_s curves resemble that of χ, with a generally increasing trend and reaching a maximum at 2.8 Ma. (ii) In general, B_{cr} and B_c and the M_{rs}/M_s and B_{cr}/B_c ratios vary with a decreasing trend, and they reach minima at 2.6 Ma rather than 2.8 Ma. (iii) There are significant differences in the amplitudes of fluctuation of these parameters. During interval III, from 8.1 to 6.8 Ma, χ, M_{rs} and M_s exhibit small amplitude fluctuations with a slightly increasing trend, while B_{cr} and B_c and their ratio exhibit larger amplitude fluctuations with a distinct increase. During interval II, all these parameters vary synchronously with large amplitude fluctuations. In contrast to interval III,

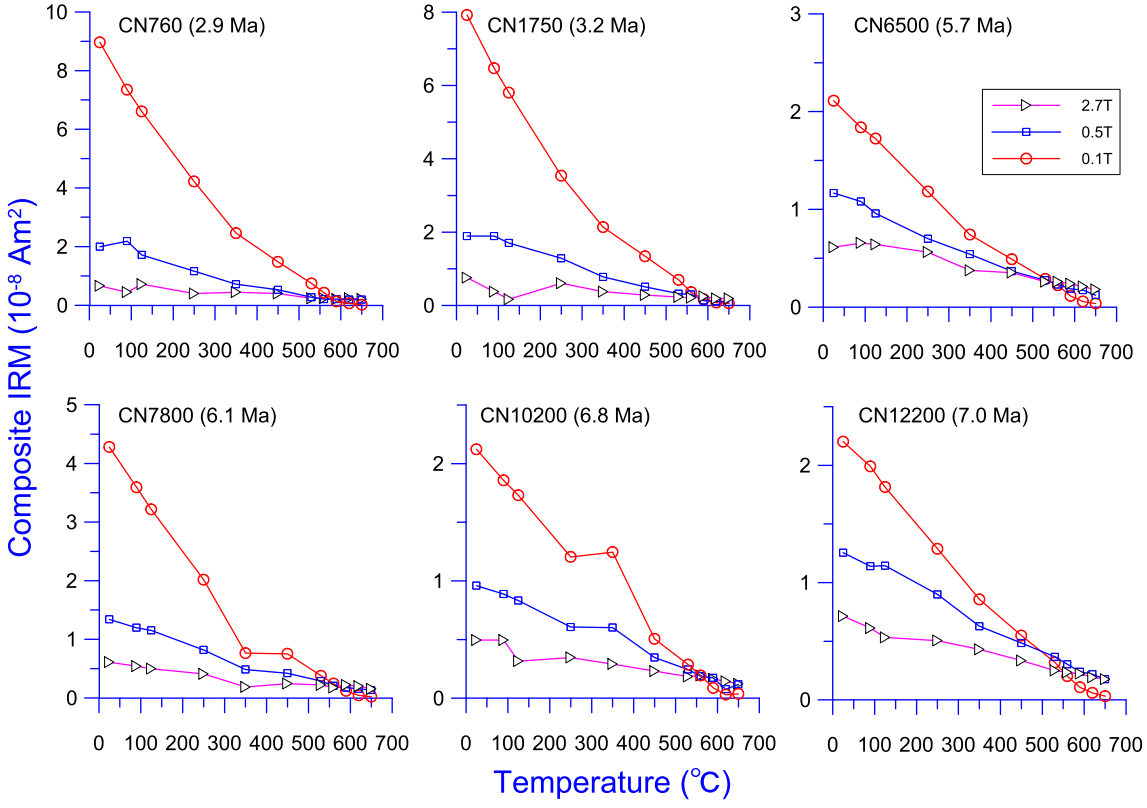

Fig. 6. Thermal demagnetization curves of a three-component IRM of selected samples from the Chaona section.

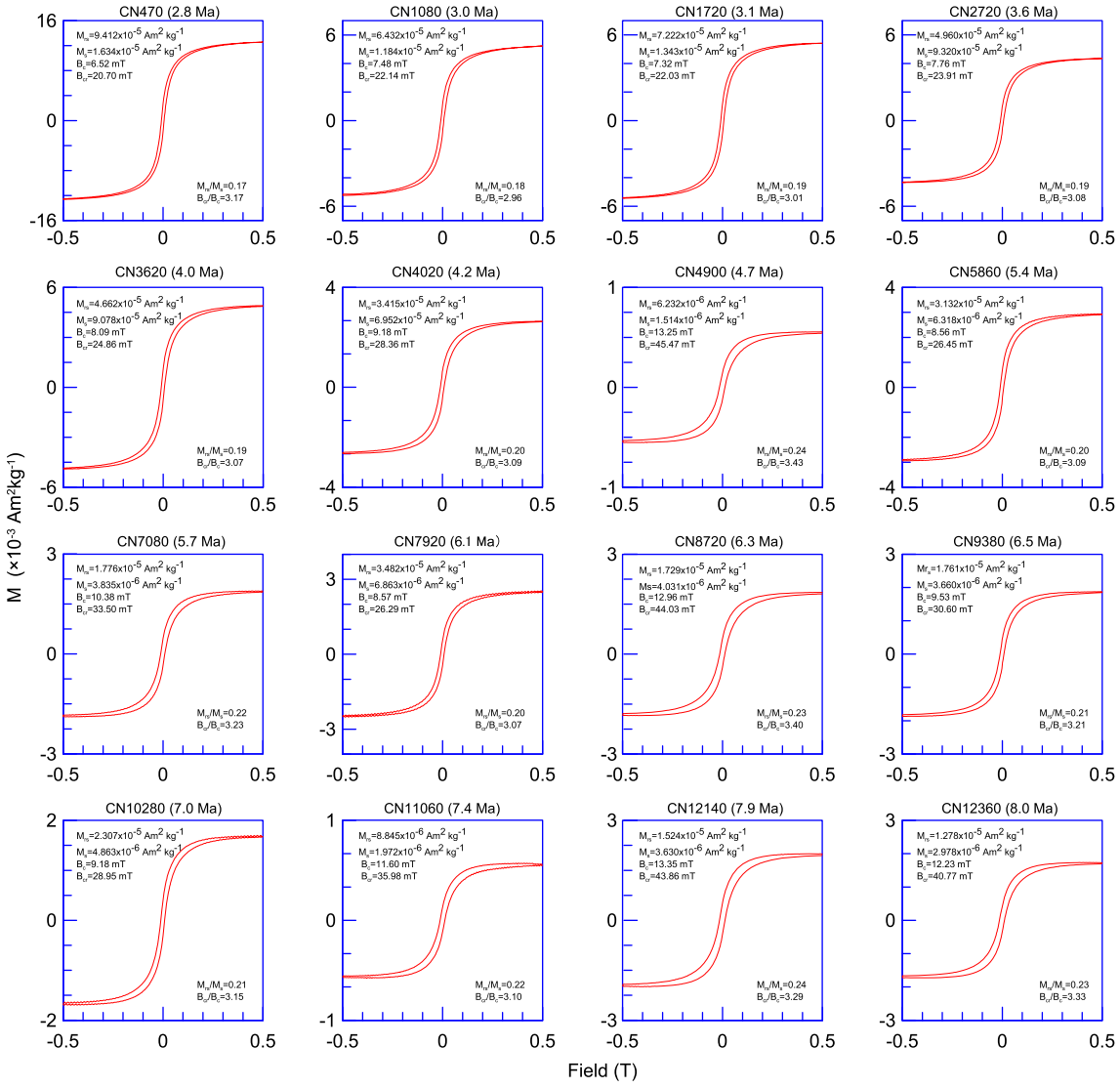

Fig. 7. Magnetic hysteresis loops of selected samples from the Chaona red clay sequence. All loops are corrected for the paramagnetic component.

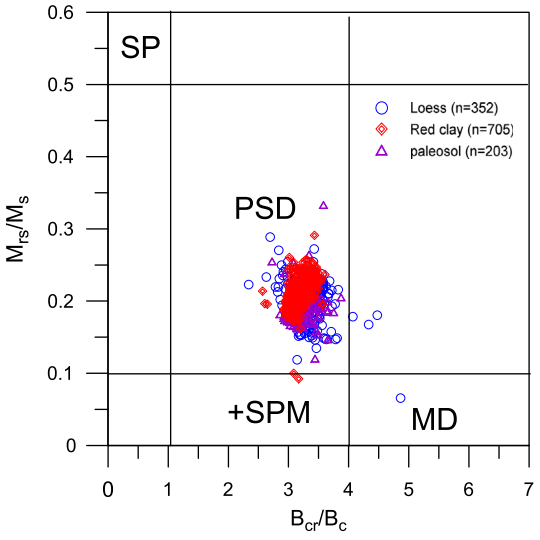

Fig. 8. Day plots for red clay (rhombuses), and Quaternary loess (circles) and paleosol (triangles) samples from the Chaona section. The data for the loess and paleosol samples are from Y.G. Song et al. (2014b).

interval I exhibits a stepwise increase in M_{rs} and M_s and a gradual decrease in B_{cr} and B_c and their ratios. In other words, the changes in magnetization and coercivity are not completely synchronous. (iv) S-ratio provides a rapid method of estimating the proportion of high coercivity magnetic minerals to low coercivity magnetic minerals; values close to 1.0 indicate a high proportion of magnetite, whereas lower values indicate an increasing proportion of hematite and goethite (King and Channell, 1990; Thompson and Oldfield, 1986). The S-ratio curve of the Chaona red clay section increases from 8.1 to 2.6 Ma, suggesting a long-term increase in the proportion of ferrimagnetic minerals relative to antiferromagnetic minerals. From 8.1 Ma to 6.8 Ma antiferromagnetic minerals such as hematite are well represented, while from 6.8 Ma to 4.3 Ma, there are systematic fluctuations in the relative amounts of ferrimagnetic mineral and antiferromagnetic minerals. After 4.3 Ma, the primary magnetic carriers are magnetite and/or maghemite (Fig. 9).

5. Discussion

5.1. Paleoclimatic significance of the magnetic parameters

The results of thermomagnetic, IRM acquisition and demagnetization, and hysteresis loops analyses indicate that the magnetic mineral

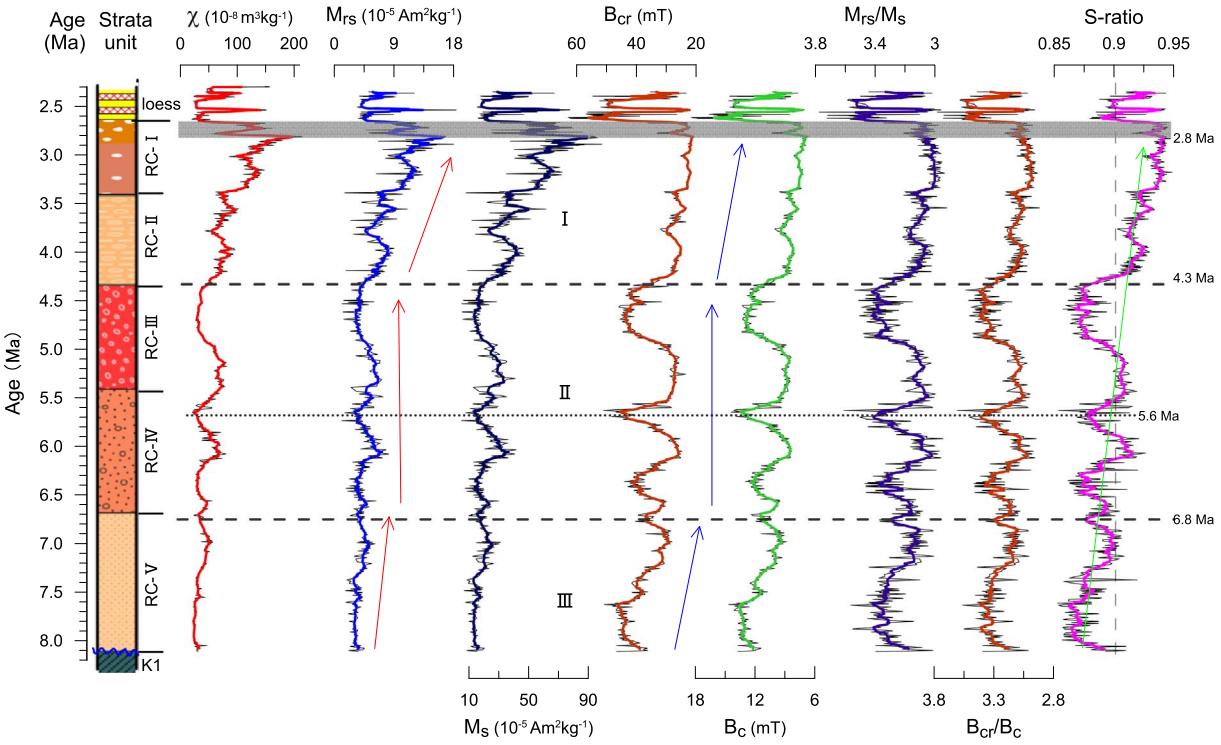

Fig. 9. Time series of selected magnetic parameters and interparametric ratios for the Chaona red clay section. The bold lines are 7-point running averages.

assemblages of the red clay of the Chaona section comprise magnetite, maghemite and hematite, which is in accord with comparable studies at Xifeng (Liu et al., 2001a, 2003), Baoji (Zhu et al., 1996) and Jiaxia (Qiang et al., 2005); however, the results of thermal demagnetization of a three-component IRM also reveal the presence of goethite. Therefore, the magnetic mineral assemblages are also similar to those of the Quaternary loess-paleosol sequence of the CLP (Heller and Liu, 1984; Liu et al., 2005, 2007; Maher, 2016).

Previous rock magnetic research on the red clay sequence convincingly demonstrates the occurrence of a magnetic enhancement mechanism similar to the overlying loess-paleosol sequence (Nie et al., 2007), which is caused primarily by the production of fine-grained ferrimagnetic grains during pedogenesis (Nie et al., 2007; Zhou et al., 1990); however, the magnetic minerals in the former have undergone a higher degree of oxidation than in the latter (Nie et al., 2007, 2016). In addition, the magnetic susceptibility of the red clay sequence is regarded as a proxy index of the intensity of the EASM (An, 2000; An et al., 2001) or precipitation intensity (Nie et al., 2008c; Sun et al., 2010). Both magnetic susceptibility and magnetization intensity (M_{rs}, M_s) reflect the concentration of magnetic minerals, especially ferrimagnetic minerals, and therefore there is a strong linear correlation among them (Fig. 10). The increased precipitation associated with a strong EASM promotes weathering and pedogenesis which results in the production of more fine magnetic grains. Therefore, M_{rs} and M_s can also be regarded as proxies of precipitation intensity. However, the relationship between magnetic susceptibility and B_c and B_{cr} is more complex, since it is non-linear (Fig. 10). When the values of magnetic susceptibility are $< 60 \times 10^{-8}\ m^3\ kg^{-1}$, the increasing coercivity (B_{cr}, and B_c) values imply the decreased influence of ferrimagnetic grains produced during pedogenesis, and thus the magnetic properties are dominated by antiferromagnetic minerals with a high coercivity.

Although both hematite and goethite are antiferromagnetic minerals, they have different paleoclimate implications. Hematite forms mainly in strongly oxidizing soils in subtropical and tropical zones under warm and dry conditions, forming from ferrihydrite via a dehydration-rearrangement process. In contrast, goethite is favored by moist conditions and forms directly from any Fe source via solution (Ji et al., 2004). Cooler and more humid climatic conditions favor the transformation of hematite to goethite which is associated with a soil color change from red to yellowish brown (Schwertmann, 1971). On the CLP, where the soils are uniformly well drained, hematite and goethite concentrations are related to a combination of soil temperature and precipitation (Ji et al., 2002; Liu et al., 2006; Maher, 1998), with hematite being favored over goethite as dryness and/or temperature increases. In addition, unlike hematite, goethite is favored under humidity conditions, and therefore in the loess sections of the CLP the hematite/goethite (Hm/Gt) ratio has been used as an indicator of dryness/humidity, hence of variations in the East Asian Monsoon (Ji et al., 2002, 2004).

We did not use diffuse reflectance spectroscopy (DRS) or other measurements to quantify the concentrations of hematite and goethite. However, qualitative estimates of their concentrations can be made from the rock magnetic analyses. The heating limb of the χ–T curves of the samples from the middle part of the section (Fig. 4) continues to decrease beyond the Curie temperature of magnetite (580 °C), and the susceptibility remains above zero even at 700 °C. This indicates the significant presence of antiferromagnetic material, which is most probably hematite because there is no indication of goethite between 80 and 120 °C in the hard component of the composite IRM (Fig. 6). The significant occurrence of hematite implies warm and dry climatic conditions in part II of the section (Fig. 11). In contrast, the occurrence of goethite, as inferred from the hard component of the composite IRM (Fig. 6), suggests that the upper (I) and lower (IV) parts of the red clay sequence were formed in a relatively humid environment.

However, the presence of goethite could be related to selective dissolution, or to the input of aeolian goethite, and/or the neoformation of goethite through pedogenesis (Liu et al., 2006). DRS analyses show that the concentration of both hematite and goethite are high in paleosols and lower in loess (Ji et al., 2004), suggesting that warm and humid interglacials are conducive to goethite transformation and formation during pedogenesis. A warm, humid environment also favors the formation of pedogenically-produced fine ferrimagnetic grains,

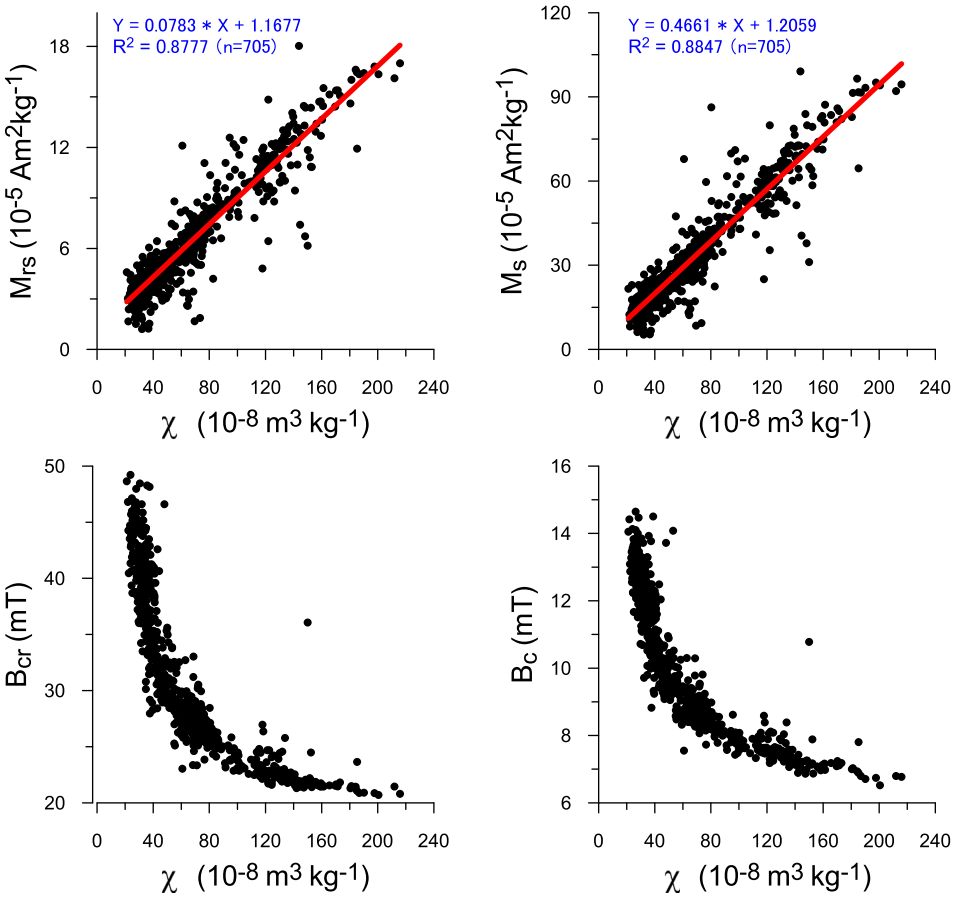

Fig. 10. Relationships between magnetic susceptibility (χ) and magnetization intensity (M_{rs}, M_s) and coercivity (B_{cr}, B_c) for the Chaona red clay section.

which cause magnetic susceptibility enhancement, with paleosols always having a higher magnetic susceptibility. If this situation is applicable to the Chaona red clay sequence, then intervals I and II should have higher magnetic susceptibility values; however, interval III has lower susceptibility values. Therefore, the occurrence of goethite may be the result of detrital inputs by strong winds in the lower part of the sequence, which is consistent with a previous interpretation that hematite and goethite in Miocene aeolian sediments were transported from the Gobi Desert by the EAWM (Hao et al., 2009).

The bulk grain-size of aeolian sediments is closely related to the wind intensity and therefore the grain-size of the deposits of the CLP is regarded as a proxy of the intensity of the EAWM (An et al., 2001; Sun et al., 2010; Sun et al., 2006). In principle, when the winter monsoon is intensified, the grain size becomes coarser and the accumulation rate of the aeolian sediments increases, which in turn results in an increase in the proportion of antiferromagnetic minerals. However, in the Chaona section the coarse fraction content (> 30 μm) varies asynchronously with the S-ratio and B_c during periods III and II (Fig. 11) and the reasons for this need further investigation.

5.2. Late Neogene evolution of the East Asian monsoon

Although the history of the EAM has been reconstructed from various proxies, the nature of the coupled relationship between the EASM and EAWM prior to the Pleistocene remains poorly constrained. To reconstruct the evolution of the EAM during the late Neogene, we selected magnetic susceptibility, M_s, B_{cr} and S-ratio as representative rock magnetic parameters and combined them with previously published grain size (Han et al., 2011; Lü et al., 2001), carbonate (Chen et al., 2007) and pollen records (Ma et al., 2005) from the Chaona red clay sequence; we also compared them with a CLP summer monsoon (SM) intensity index (Sun et al., 2010) (Fig.11). The carbonate content (Chen et al., 2007; Sun et al., 2010) and magnetic susceptibility (An, 2000; An et al., 2001; Nie et al., 2008c; Sun et al., 2010) of aeolian red clay sediments from the CLP are regarded as reliable indicators of effective precipitation and the intensity of the EASM, and grain size is usually used as an indicator of wind strength (Sun et al., 2006; Vandenberghe et al., 2004) or the intensity of the EAWM (Lü et al., 2001; Sun et al., 2010). The records of magnetic susceptibility (χ), M_{rs}, M_s and S-ratio for the Chaona red clay section exhibit a long-term stepwise increasing trend (Figs. 9, 11), which can be interpreted as reflecting a gradual intensification of the EASM. In addition, the coercivity (B_{cr}, B_c) records can be divided into two well-defined intervals: (i) from 8.1 to 4.3 Ma they exhibit three large amplitude cycles, and (ii) after 4.3 Ma the cycles are of significantly lower amplitude. These differences may indicate changes in the formation mechanism of antiferromagnetic minerals and pronounced fluctuations in the East Asian environment.

From the variations in magnetic properties and bulk sediment grain-size, the climatic evolution between 8.1 and 2.6 Ma can be divided into 3 intervals (Fig. 11), which are described below.

Interval III (8.1–6.8 Ma) corresponds to lithological unit V which consists of yellowish-brown paleosols with scattered carbonate nodules and has the weakest degree of pedogenesis in the entire red clay sequence. χ and M_s are both relatively low and uniform with a small peak at 7.0 Ma, suggesting weak pedogenesis. During this interval, the calcite record (Fig. 11) suggests relatively low precipitation and weak seasonality (Chen et al., 2007). Pollen assemblages indicate that the vegetation was grassland with scattered broadleaved trees (Ma et al., 2005) (Fig. 11), suggesting a moist, sub-humid climate. Evidently, the relatively lower temperature and precipitation conditions were insufficient to produce a significant amount of fine-grained magnetic grains during pedogenesis, and therefore that the summer monsoon was relatively weak. The S-ratio and B_{cr} curves are concave within the interval, suggesting that the antiferromagnetic mineral content decreased

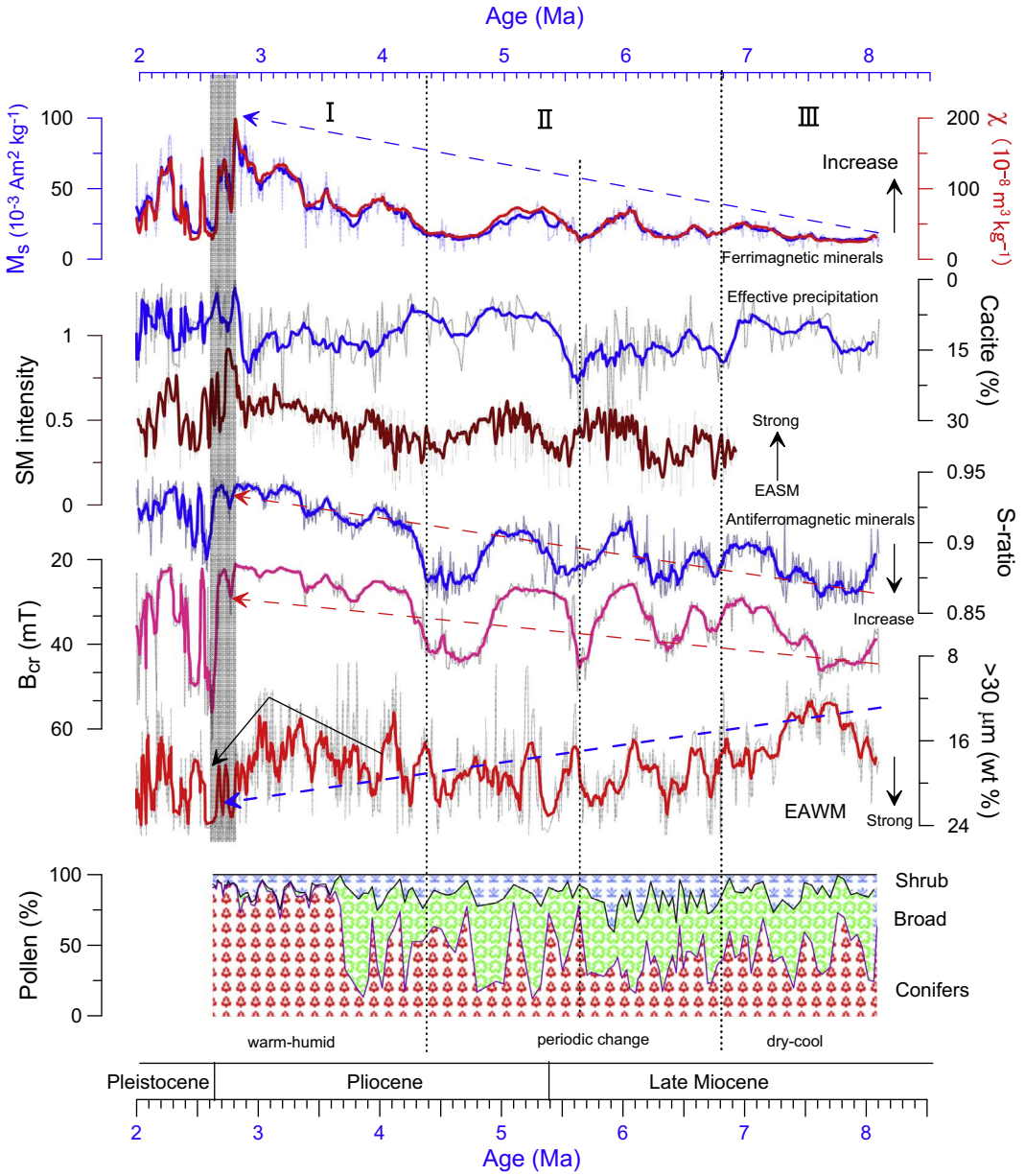

Fig. 11. East Asian climatic evolution during the Late Miocene and Pliocene recorded by various proxies from the Chaona red clay section. The calcite record is from Chen et al. (2007), the SM (Summer Moonsoon) intensity record is from Sun et al. (2010), and the grain size (> 30 μm) record is from Lü et al. (2001). Bold line of SM intensity is 15-point running averages, and the other bold lines are 7-point running averages.

after 8.1 Ma, reached a minimum 7.6 Ma, and then increased rapidly, which is consistent with the long-period cycles evident in the content of coarse grained material (> 30 μm). These oscillations suggest cyclic fluctuations in wind intensity, hence of the winter monsoon.

Interval II (6.8–4.3 Ma) corresponds to lithological units IV and III. The most prominent characteristic of this interval is that all the magnetic proxies exhibit two major cycles with minima/maxima at around 5.6 Ma, although there are also some minor fluctuations during the interval from 6.8 to 6 Ma (Fig. 9). This is interpreted as reflecting periodic changes in both the EASM and EAWM, which is consistent with the summer monsoon intensity proxy of the CLP (SM) (Fig. 11). The interval can be subdivided lithologically into two stages: (i) From 6.8 to 5.6 Ma, it consists of light brown-red paleosols with scattered small carbonate nodules. χ, M_s, SM intensity and S-ratio generally exhibit synchronous low amplitude fluctuations, indicating weak cyclical variations in the summer monsoon. In addition, the carbonate content is higher than during the interval of strata unit III, suggesting that effective precipitation was lower. B_{cr} and grain size (> 30 μm) exhibit two well-defined, high amplitude cycles, and the fluctuations in antiferromagnetic mineral content may reflect variations in wind intensity; these characteristics suggest that the winter monsoon was still strong. The magnetic, carbonate and grain-size proxies suggest a cool, dry climate. (ii) From 5.6 to 4.3 Ma, although the sediments are dark-reddish-brown color with well-developed Fe–Mn coatings and scattered large carbonate nodules, indicating the highest degree of pedogenesis of the entire section, the magnetic parameters exhibit only intermediate values. There are two possible interpretations for these lower values. One is that it may be the result of widespread gleying under reducing soil conditions (Ding et al., 1999) during which the magnetic minerals may have been affected or destroyed (Liu et al., 2001b). The other possibility is that the formation of maghemite and hematite is non-linearly correlated to the amount of precipitation with a threshold about 1200 mm/yr (Han et al., 1996). Below this threshold, a positive correlation is observed, which is valid typically for the loess/paleosol

sequences (Maher, 2016; Y. Song et al., 2014a). But for the red-clay sequence, if there are superabundant precipitation (> 1200 mm/yr), an opposite correlation could be true, with further increasing precipitation, both χ and hematite content will decrease. The calcite content is uniformly low, possibly reflecting a warmer and moister climate (Chen et al., 2007). Various magnetic parameters exhibit an addition cycle, and the > 30 μm grain-size content is relatively high and stable. The dust flux in the North Pacific reached a minimum from about 5.4–4.4 Ma, indicating a relatively moist Asian interior (Rea et al., 1998). In summary, the climate was characterized by both a stronger EASM and a relatively strong and stable EAWM.

Interval I (4.3–2.6 Ma), corresponding to lithological units II and I. χ, M_s and the SM index exhibit a stepwise increase which continues until 2.8 Ma; thus there was a significant intensification of the summer monsoon. S-ratio and B_{cr} respectively exhibit a steep increase and decrease at the beginning of the interval, followed by more subdued fluctuations until 2.6 Ma (Fig. 11). In contrast, the > 30 μm grain-size content exhibits high frequency oscillations between 4.3 and 3.3 Ma. From 3.3–2.6 Ma, the sediments are brownish-red in color and are strongly weathered with Fe and Mn skins and a prismatic structure. The pollen assemblages suggest typical Cupressaceae forest and in addition the xerophytic *Artemisia* disappears (Fig. 11). These characteristics suggest a relatively warm and humid climate during the late Pliocene (Wu et al., 2007), consistent with the late Pliocene warm period, and hence a significantly intensified summer monsoon. At the same time, the > 30 μm grain content increases continuously from 3.3 to 2.6 Ma (Fig. 11), indicating the intensification of the winter monsoon; this is consistent with an abrupt increase in the aeolian mass accumulation rates in North Pacific in the late Pliocene (Rea et al., 1998) and with the coeval increase in global ice volume (Zachos et al., 2008).

The interval from 2.8 to 2.6 Ma (indicating by shading in Figs. 9, 11) is an important climatic transitional period from the relatively warm Pliocene to the glacial-interglacial cold-warm oscillations of the Pleistocene. Both the > 30 μm grain-size content and the magnetic parameters exhibit abrupt, high amplitude changes around 2.8–2.6 Ma. All of the EASM proxies, including χ, M_s, carbonate content and SM index, reach their maxima at around 2.8 Ma, and then decrease abruptly at around 2.6 Ma, suggesting that the climate became cooler and drier and/or that there was a major reorganization of the pattern of atmospheric circulation (Ding et al., 2000). Sea surface temperatures (SST) estimated from the organic $U^{k'}_{37}$ proxy at ODP Site 1208 in the North Pacific (Herbert et al., 2016) also decreased rapidly. We conclude that both the summer and winter monsoons strengthened during this interval, against a background of increasing global ice volume (Zachos et al., 2008) (Fig.11). Under the climatic transitional period, pedogenesis gradually transferred from the 'red-clay' model (high degree of pedogenesis) to 'loess-paleosol' model (moderate to low degree of pedogenesis), the effective precipitation could affect the pedogenesis model, which caused the asynchronous changes of various parameters (χ, a*, grain size, M_{rs}, B_{cr} etc) (Figs.2, 9, 11). In other words, the relationships among these parameters could be either positively correlated, or negatively correlated depending on the exact amount of precipitation.

5.3. Possible climatic driving mechanisms

It is important to understand the forcing mechanisms of Mio-Pliocene climate change, especially during the Pliocene warm period which may provide an analogue for a future warmer Earth (Haywood et al., 2016). However, the main drivers and mechanisms of East Asian climatic evolution during the Neogene are hotly debated. Four major factors have been suggested: global cooling (Ao et al., 2016; Lu and Guo, 2014; Lu et al., 2010; Miao et al., 2011), uplift of the Tibetan Plateau (An et al., 2001; Song et al., 2007; Sun et al., 1998b), retreat of the Paratethys Sea (Zhang et al., 2007), and the gradual closure of the Panama Seaway (Driscoll and Haug, 1998; Nie et al., 2014b). The first two factors are considered the most important drivers in the EAM area.

Geological evidence and climate simulations indicate that the uplift of the Tibetan Plateau had a profound impact on the initiation and development of the climate of East Asia. The altitude and extent of the Tibetan Plateau can affect moisture transport from the ocean to the Asian interior, as well as the thermal contrast between land and sea, thereby altering large-scale patterns of atmospheric circulation and causing climate change in East Asia (An et al., 2001; Kutzbach et al., 1989; Liu and Dong, 2013). However, the timing, amplitude and extent of Tibetan Plateau uplift or growth have long been debated. Numerical experiments indicate that Paratethys retreat could have strengthened the East Asian monsoon and greatly increased the humidity and aridity in monsoon areas and in Northwest China, respectively (Ramstein et al., 1997; Zhang et al., 2007), which is similar to the impact of Tibetan Plateau uplift on East Asian climate (Ramstein et al., 1997). The progressive closure of the Panama Seaway in the late Miocene and early Pliocene increased thermohaline circulation and enhanced moisture supply to the Eurasian continent, but it can only explain a short-duration shift in EASM intensity within the Pliocene (Ao et al., 2016; Nie et al., 2008c, 2014b).

More recently, global cooling has come to be regarded as the major driver of climate change in Asia during the late Cenozoic, and geological and paleontological evidence suggests that it had a significant influence on the Asian monsoon (Ao et al., 2016; Lu and Guo, 2014; Lu et al., 2010; Miao et al., 2011). Global cooling, associated with the expansion of global ice volume indicated by the marine oxygen isotope record, would have strengthened the Siberian-Mongolian High thereby reinforcing the winter monsoon circulation. In addition, a colder climate would reduce moisture transport by the Asian monsoon circulation, causing aridification in East Asia (Guo et al., 2004; J. Li et al., 2014b; Lu et al., 2010). Ao et al. (2016) attributed the long-term trend increasing EASM strength during the late Neogene to progressive Antarctic glaciation, which would have intensified the cross-equatorial pressure gradient between an atmospheric high-pressure cell over Australia and a low-pressure cell over mid-latitude East Asia, as well as intensifying the cross-equatorial sea-surface temperature gradient. These combined atmospheric and oceanic adjustments may have led to a strengthened EASM. Climate model simulations indicate that the Late Pliocene growth of the West Antarctic ice sheet may have caused a strongly enhanced cross-equatorial pressure gradient, although there was no significant increase in simulated averaged EASM precipitation. Consequently, it is difficult to explain the simultaneous enhancement of both the EASM and EAWM during Interval I, or the Pliocene warm period. For example, magnetic properties and other evidence for strong pedogenesis indicate considerably increased EASM precipitation during the Pliocene (An et al., 2001; Ding et al., 1999; Nie et al., 2008a, 2010a, 2013; Y.G. Song et al., 2014b; Sun et al., 1998b).

To examine the relationship between East Asian climate and global cooling, we compared the various proxies from the Chaona red clay section with a global oxygen isotope record (Fig. 12). Compared to the global oxygen isotope, there are striking differences in the overall trends of the various proxies during this interval from 4.3 to 2.8/2.6 Ma. The > 30 μm grain-size content (violet curve) exhibits a similar long-term trend to global ice volume (blue curve) from 8.1 to 2.5 Ma, although the amplitude and detailed patterns of variability are different. Increases in the > 30 μm grain-size content roughly correspond to increased ice volume, indicating that global ice volume and global cooling may have driven the long-term evolution of the EAWM. However, the magnetic parameters covary directly with global ice volume only during the period from 8.1 to 4.3 Ma, and especially after 6.0 Ma, which corresponds to the expansion of the Western Antarctic Ice Sheet (WAIS) (Zachos et al., 2008). However, they exhibit the opposite pattern of variation during interval I, from 4.3 to 2.6 Ma. If global cooling were the primary driver of EASM evolution during the Pliocene, the climate would be expected to have been cool and dry; however, the magnetic parameters and pollen assemblages suggest a warm and

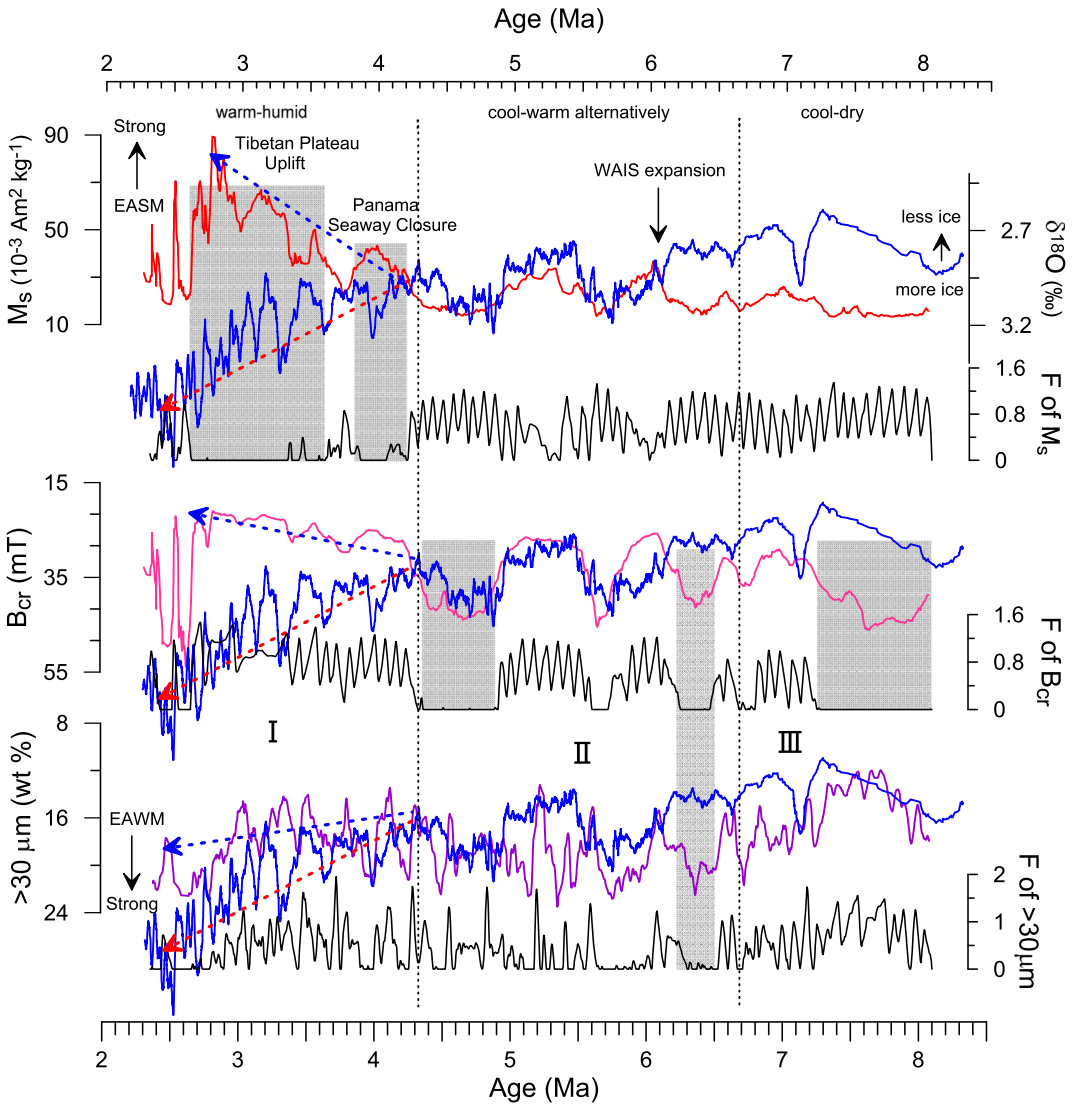

Fig. 12. Comparison of magnetic parameters (M_s: upper; B_{cr}: middle; 7-point running averages) and > 30 μm grain-size (lower; 11-point running averages) for the Chaona red clay section with global ice volume (blue line; 31-point running averages) (Zachos et al., 2008) and with major climatic and tectonic events during the Late Neogene. The simulation results F parameter, calculated using AnalySeries 2.08 (Paillard and Parrenin, 2004), is also shown. (For interpretation of the references to color in this figure legend, the reader is referred to the web version of this article.)

humid environment. In addition, there is a gradually increasing divergence between the > 30 μm grain-size content and the global oxygen isotope record (Fig. 12), which is difficult to explain in terms of global ice volume forcing of the EAWM.

Here, we attempt to introduce a global ice volume-insolation-atmospheric CO_2 model (Paillard and Parrenin, 2004) to verify the relationship between East Asian climatic change and global ice volume. The conceptual model is based on three variables: global ice volume (V) forced both by Northern Hemisphere summer insolation (I) and atmospheric pCO_2 (C); extent of the Antarctic ice sheet (A) forced by sea level changes; and atmospheric CO_2 linked primarily to deep-water state, glacial or interglacial. The F parameter is used to assess if the ocean is in an interglacial (F < 0) or glacial (F > 0) states which increases with V and decreases with A, C and I (see details in Paillard and Parrenin, 2004). The AnalySeries software package (Paillard et al., 1996) enables F values to be counted with insolation as a replaceable variable. If the East Asian climate is driven by global ice volume, the magnetic parameters of the red clay sediments should have inherent relationships with V, A and C. We substituted the climate proxies from the Chaona red clay section for insolation, and in this case the F parameter can preliminarily be regarded as reflecting the degree of coupling between East Asian climatic proxies and global cooling. We find that the F parameter varies systematically (shaded areas in Fig. 12). For the M_s substitution, we can observe two intervals with values of zero, 4.3–3.8 Ma and 3.6–2.6 Ma, which are well correlated with high M_s values, indicating a warm and humid interglacial climate. For the B_{cr} substitution, the intervals are from 8.1–7.3 Ma, 6.5–6.3 Ma and 4.9–4.3 Ma; these intervals generally have a high coercivity, indicating a strongly reducing environment. For the grain-size substitution, there are no obvious steps, indicating a close relationship with global cooling. Although the application of this model to continental deposits needs to be further investigated, it may help to evaluate the possible contribution of global cooling to climate in East Asia during the late Cenozoic. At a minimum, it appears to indicate that global cooling may not have been the primary driver of East Asian climate especially for the EASM during the Pliocene.

We attribute the enhancement of the East Asian monsoon, especially the EASM, primarily to tectonic events. Closure of the Panama Seaway around 4.5 Ma (Haug et al., 2001) intensified the Gulf stream which transported more moisture to higher latitudes in the North Atlantic. Climate simulation results (Motoi and Chan, 2010) show that the closure can alter the patterns of temperature and salinity distribution in

the Pacific Ocean, intensify the EASM, and thus cause more precipitation in the CLP (Nie et al., 2008b, 2013, 2014b). The accelerated uplift of the Tibetan Plateau since 3.6 Ma may have played an important role in intensifying both the EASM and EAWM. Late Pliocene uplift of the Tibetan Plateau would have increased the sea–land pressure gradient, resulting in increased precipitation in the CLP (An et al., 2001). We thus conclude that late Neogene East Asian climate changes occurred in the context of global cooling, and that regional tectonic forcing would have affected the local and regional climate and environment. More tentatively, global cooling may have had a greater effect on the EAWM than on the EASM.

6. Conclusions

Detailed rock magnetic analysis indicates that the main magnetic minerals in the red clay of the Chaona section are magnetite, maghemite, hematite and goethite, similar to the overlying Quaternary loess-paleosol sequence. The rock magnetic stratigraphy, combined with other proxy climate records, reveals a stepwise intensification of the summer monsoon and a persistent enhancement of the winter monsoon in East Asia during the Late Neogene from 8.1 to 2.6 Ma. The climatic record can be subdivided into three intervals: interval III, from 8.1 to 6.8 Ma, when the climate was cool and dry and both the EASM and EAWM were relatively weak; interval II, from 6.8 to 4.3 Ma, when the climate was characterized by cool-warm oscillations; and interval II, from 4.3 to 2.8/2.6 Ma, when the climate was warm and humid and the EASM rapidly strengthened while the EAWM fluctuated widely with an increasing trend. We conclude that prior to 4.3 Ma the evolution of both the EASM and EAWM was related to global cooling. We attribute the intensified EASM during the late Pliocene to global tectonic events such as the gradual closure of the Panama Seaway and the uplift of the Tibetan Plateau.

Acknowledgments

We greatly appreciate the constructive suggestions and comments from the editors Thomas Algeo and Hanlie Hong and anonymous reviewers. We are grateful to Cor Langereis, Mike Dekker, Guillaume Dupont-Nivet, Zhihong Gong, Fuli Wu, Kaodao Fu, Liangqing Lü for laboratory guidance and field help. We would like to thank Prof. Jan Bloemendal for his good suggestions and language polishing. This work was supported by Natural Science Foundation of China (NSFC) (nos: 41290253, 41572162, 41472147), Xi'an Centre of Geological Survey, CGS (CGS Diaosheng [2017]0438), International partnership Program of Chinese Academy of Sciences (CAS) (no: 132B61KYS20160002) and Scientific and Technological Innovation Team of CAS (no: CAS Renzi (2013)47).

References

Alonso-Zarza, A.M., Zhao, Z., Song, C.H., Li, J.J., Zhang, J., Martín-Pérez, A., Martín-García, R., Wang, X.X., Zhang, Y., Zhang, M.H., 2009. Mudflat/distal fan and shallow lake sedimentation (upper Vallesian–Turolian) in the Tianshui Basin, Central China: evidence against the late Miocene eolian loess. Sediment. Geol. 222, 42–51.

An, Z.S., 2000. The history and variability of the East Asian paleomonsoon climate. Quat. Sci. Rev. 19, 171–187.

An, Z.S., Liu, T.S., Lu, Y.C., Porter, S.C., Kukla, G., Wu, X.H., Hua, Y.M., 1990. The long-term paleomonsoon variation recorded by the loess-paleosol sequence in Central China. Quat. Int. 7-8, 91–95.

An, Z.S., Kukla, G.J., Porter, S.C., Xiao, J.L., 1991. Magnetic susceptibility evidence of monsoon variation on the Loess Plateau of central China during the last 130,000 years. Quat. Res. 36, 29–36.

An, Z.S., Kutzbach, J.E., Prell, W.L., Porter, S.C., 2001. Evolution of Asian monsoons and phased uplift of the Himalaya–Tibetan plateau since Late Miocene times. Nature 411, 62–66.

Ao, H., Roberts, A.P., Dekkers, M.J., Liu, X., Rohling, E.J., Shi, Z., An, Z., Zhao, X., 2016. Late Miocene–Pliocene Asian monsoon intensification linked to Antarctic ice-sheet growth. Earth Planet. Sci. Lett. 444, 75–87.

Bloemendal, J., Liu, X.M., Rolph, T.C., 1995. Correlation of the magnetic-susceptibility stratigraphy of Chinese Loess and the marine oxygen-isotope record - chronological and paleoclimatic implications. Earth Planet. Sci. Lett. 131, 371–380.

Chen, J., Chen, Y., Liu, L., Ji, J., Balsam, W., Sun, Y., Lu, H., 2006. Zr/Rb ratio in the Chinese loess sequences and its implication for changes in the East Asian winter monsoon strength. Geochim. Cosmochim. Acta 70, 1471–1482.

Chen, X., Fang, X., An, Z., Han, W., Wang, X., Bai, Y., Hong, Y., 2007. An 8.1 Ma calcite record of Asian summer monsoon evolution on the Chinese central Loess Plateau. Sci. China Ser. D Earth Sci. 50, 392–403.

Day, R., Fuller, M., Schmidt, V.A., 1977. Hysteresis properties of titanomagnetites: grain-size and compositional dependence. Phys. Earth Planet. Inter. 13, 260–267.

Deng, C., Zhu, R., Verosub, K.L., Singer, M.J., Vidic, N.J., 2004. Mineral magnetic properties of loess/paleosol couplets of the central loess plateau of China over the last 1.2 Myr. J. Geophys. Res. Solid Earth 109, B01103. http://dx.doi.org/10.01029/02003JB002532.

Ding, Z., Sun, J., Yang, S., Liu, T., 1998. Preliminary magnetostratigraphy of a thick eolian red clay-Loess sequence at Lingtai, the Chinese Loess Plateau. Geophys. Res. Lett. 25, 1225–1228.

Ding, Z.L., Xiong, S.F., Sun, J.M., Yang, S.L., Gu, Z.Y., Liu, T.S., 1999. Pedostratigraphy and paleomagnetism of a similar to 7.0 Ma eolian loess-red clay sequence at Lingtai, Loess Plateau, north-central China and the implications for paleomonsoon evolution. Palaeogeogr. Palaeoclimatol. Palaeoecol. 152, 49–66.

Ding, Z.L., Rutter, N.W., Sun, J.M., Yang, S.L., Liu, T.S., 2000. Re-arrangement of atmospheric circulation at about 2.6 Ma over northern China: evidence from grain size records of loess-palaeosol and red clay sequences. Quat. Sci. Rev. 19, 547–558.

Driscoll, N.W., Haug, G.H., 1998. A short circuit in thermohaline circulation: a cause for northern hemisphere glaciation? Science 282, 436–438.

Dunlop, D.J., Özdemir, Ö., 1997. Rock Magnetism: Fundamentals and Frontiers. Cambridge Univ. Press, New York.

Dupont-Nivet, G., Krijgsman, W., Langereis, C.G., Abels, H.A., Dai, S., Fang, X., 2007. Tibetan plateau aridification linked to global cooling at the Eocene-Oligocene transition. Nature 445, 635–638.

Evans, M.E., Heller, F., 2001. Magnetism of loess/palaeosol sequences: recent developments. Earth Sci. Rev. 54, 129–144.

Fang, X., Zan, J., Appel, E., Lu, Y., Song, C., Dai, S., Tuo, S., 2015. An Eocene-Miocene continuous rock magnetic record from the sediments in the Xining Basin, NW China: indication for Cenozoic persistent drying driven by global cooling and Tibetan Plateau uplift. Geophys. J. Int. 201, 78–89.

Fukuma, K., Torii, M., 1998. Variable shape of magnetic hysteresis loops in the Chinese loess-paleosol sequence. Earth Planets Space 50, 9–14.

Guo, Z., Liu, T., Guiot, J., Wu, N., Lü, H., Han, J., Liu, J., Gu, Z., 1996. High frequency pulses of East Asian monsoon climate in the last two glaciations: link with the North Atlantic. Clim. Dyn. 12, 701–709.

Guo, Z.T., Peng, S.Z., Hao, Q.Z., Biscaye, P.E., Liu, T.S., 2001. Origin of the Miocene-Pliocene Red-Earth formation at Xifeng in northern China and implications for paleoenvironments. Palaeogeogr. Palaeoclimatol. Palaeoecol. 170, 11–26.

Guo, Z.T., Ruddiman, W.F., Hao, Q.Z., Wu, H.B., Qiao, Y.S., Zhu, R.X., Peng, S.Z., Wei, J.J., Yuan, B.Y., Liu, T.S., 2002. Onset of Asian desertification by 22 Myr ago inferred from loess deposits in China. Nature 416, 159–163.

Guo, Z.T., Peng, S.Z., Hao, Q.Z., Biscaye, P.E., An, Z.S., Liu, T.S., 2004. Late Miocene-Pliocene development of Asian aridification as recorded in the Red-Earth Formation in northern China. Glob. Planet. Chang. 41, 135–145.

Han, J., Lü, H., Wu, N., Guo, Z., 1996. The magnetic susceptibility of modern soils in China and its use for paleoclimate reconstruction. Stud. Geophys. Geod. 40, 262–275.

Han, W., Fang, X., Berger, A., Yin, Q., 2011. An astronomically tuned 8.1 Ma eolian record from the Chinese Loess Plateau and its implication on the evolution of Asian monsoon. J. Geophys. Res. Atmos. 116, D24114. http://dx.doi.org/10.21029/22011JD016237.

Hao, Q., Guo, Z., 2007. Magnetostratigraphy of an early-middle Miocene loess-soil sequence in the western Loess Plateau of China. Geophys. Res. Lett. 34, L18305. http://dx.doi.org/10.11029/12007GL031162.

Hao, Q., Oldfield, F., Bloemendal, J., Torrent, J., Guo, Z., 2009. The record of changing hematite and goethite accumulation over the past 22 Myr on the Chinese Loess Plateau from magnetic measurements and diffuse reflectance spectroscopy. J. Geophys. Res. Solid Earth 114, B12101. http://dx.doi.org/10.11029/12009JB006604.

Haug, G.H., Tiedemann, R., Zahn, R., Ravelo, A.C., 2001. Role of Panama uplift on oceanic freshwater balance. Geology 29, 207–210.

Haywood, A.M., Dowsett, H.J., Dolan, A.M., 2016. Integrating geological archives and climate models for the mid-Pliocene warm period. Nat. Commun. 7, 10646.

Heller, F., Liu, T.S., 1982. Magnetostratigraphical dating of loess deposits in China. Nature 300, 431–433.

Heller, F., Liu, T.S., 1984. Magnetism of Chinese loess deposits. Geophys. J. R. Astron. Soc. 77, 125–141.

Herbert, T.D., Lawrence, K.T., Tzanova, A., Peterson, L.C., Caballero-Gill, R., Kelly, C.S., 2016. Late Miocene global cooling and the rise of modern ecosystems. Nat. Geosci. 9, 843–847.

Ji, J., Balsam, W., Chen, J., Liu, L., 2002. Rapid and quantitative measurement of hematite and goethite in the Chinese loess-paleosol sequence by diffuse reflectance spectroscopy. Clay Clay Miner. 50, 208–216.

Ji, J., Chen, J., Balsam, W., Lu, H., Sun, Y., Xu, H., 2004. High resolution hematite/goethite records from Chinese loess sequences for the last glacial-interglacial cycle: rapid climatic response of the East Asian Monsoon to the tropical Pacific. Geophys. Res. Lett. 31, L03207.

King, J.W., Channell, J.E.T., 1990. Sedimentary magnetism, environmental magnetism, and magnetostratigraphy. Rev. Geophys. 29, 358–370.

Kukla, G., Heller, F., Ming, L.X., Chun, X.T., Sheng, L.T., Sheng, A.Z., 1988. Pleistocene climates in China dated by magnetic susceptibility. Geology 16, 811–814.

Kutzbach, J.E., Guetter, P.J., Ruddiman, W.F., Prell, W.L., 1989. Sensitivity of climate to Late Cenozoic uplift in Southern Asia and the American West - numerical experiments. J. Geophys. Res.-Atmos. 94, 18393–18407.
Li, J., Zhang, J., Song, C., Zhao, Z., Zhang, Y., Wang, X., Zhang, J., Cui, Q., 2006. Miocene Bahean stratigraphy in the Longzhong Basin, northern central China and its implications in environmental change. Sci. China Ser. D Earth Sci. 49, 1270–1279.
Li, Y., Song, Y.G., Qian, L.B., Li, X.M., Qiang, X.K., An, Z.S., 2013. Paleomagnetic and fission-track dating of a Late Cenozoic red earth section in the Liupan Shan and associated tectonic implications. J. Earth Sci. 24, 506–518.
Li, F., Wu, N., Rousseau, D.-D., Dong, Y., Zhang, D., Pei, Y., 2014. Late Miocene–Pliocene paleoclimatic evolution documented by terrestrial mollusk populations in the Western Chinese Loess Plateau. PLoS One 9, e95754.
Li, J., Fang, X., Song, C., Pan, B., Ma, Y., Yan, M., 2014. Late Miocene–quaternary rapid stepwise uplift of the NE Tibetan Plateau and its effects on climatic and environmental changes. Quat. Res. 81, 400–423.
Liu, T.S., 1985. Loess and the Environment. China Ocean Press, Beijing, pp. 1–251.
Liu, X., Dong, B., 2013. Influence of the Tibetan Plateau uplift on the Asian monsoon-arid environment evolution. Chin. Sci. Bull. 58, 4277–4291.
Liu, X.M., An, Z.S., Rolph, T., Qiang, X.K., Hesse, P., Lu, H.Y., Zhou, J., Cai, Y.J., 2001a. Magnetic properties of the Tertiary red clay from Gansu. Sci. China Ser. D Earth Sci. 44, 635–651.
Liu, X.M., Hesse, P., Beget, J., Rolph, T., 2001b. Pedogenic destruction of ferrimagnetics in Alaskan loess deposits. Aust. J. Soil Res. 39, 99–115.
Liu, X.M., Rolph, T., An, Z., Hesse, P., 2003. Paleoclimatic significance of magnetic properties on the Red Clay underlying the loess and paleosols in China. Palaeogeogr. Palaeoclimatol. Palaeoecol. 199, 153–166.
Liu, Q.S., Deng, C.L., Yu, Y.J., Torrent, J., Jackson, M.J., Banerjee, S.K., Zhu, R.X., 2005. Temperature dependence of magnetic susceptibility in an argon environment: implications for pedogenesis of Chinese loess/palaeosols. Geophys. J. Int. 161, 102–112.
Liu, Q.S., Bloemendal, J., Torrent, J., Deng, C.L., 2006. Contrasting behavior of hematite and goethite within paleosol S5 of the Luochuan profile, Chinese Loess Plateau. Geophys. Res. Lett. 33, L20301. http://dx.doi.org/10.21029/22006GL027172.
Liu, Q., Deng, C., Torrent, J., Zhu, R., 2007. Review of recent developments in mineral magnetism of the Chinese loess. Quat. Sci. Rev. 26, 368–385.
Lowrie, W., 1990. Identification of ferromagnetic minerals in a rock by coercivity and unblocking temperature properties. Geophys. Res. Lett. 17, 159–162.
Lu, H.Y., An, Z.S., 1998. Paleoclimatic significance of grain size of loess-palaeosol deposit in Chinese Loess Plateau. Sci. China Ser. D Earth Sci. 41, 626–631.
Lu, H., Guo, Z., 2014. Evolution of the monsoon and dry climate in East Asia during late Cenozoic: a review. Sci. China Earth Sci. 57, 70–79.
Lü, L., Fang, X., Mason, J.A., Li, J., An, Z., 2001. The evolution of coupling of Asian winter monsoon and high latitude climate of Northern Hemisphere. Sci. China Ser. D Earth Sci. 44, 185–191.
Lu, H., Wang, X., Li, L., 2010. Aeolian sediment evidence that global cooling has driven late Cenozoic stepwise aridification in central Asia. Geol. Soc. Lond., Spec. Publ. 342, 29–44.
Ma, Y., Wu, F., Fang, X., Li, J., An, Z., Wang, W., 2005. Pollen record from red clay sequence in the central Loess Plateau between 8.10 and 2.60 Ma. Chin. Sci. Bull. 50, 2234–2243.
Maher, B.A., 1998. Magnetic properties of modern soils and Quaternary loessic paleosols: paleoclimatic implications. Palaeogeogr. Palaeoclimatol. Palaeoecol. 137, 25–54.
Maher, B.A., 2016. Palaeoclimatic records of the loess/palaeosol sequences of the Chinese Loess Plateau. Quat. Sci. Rev. 154, 23–84.
Miao, Y.F., Fang, X.M., Herrmann, M., Wu, F.L., Zhang, Y.Z., Liu, D.L., 2011. Miocene pollen record of KC-1 core in the Qaidam Basin, NE Tibetan Plateau and implications for evolution of the East Asian monsoon. Palaeogeogr. Palaeoclimatol. Palaeoecol. 299, 30–38.
Motoi, T., Chan, W.-L., 2010. Colder Subarctic Pacific with larger sea ice caused by closure of the Central American Seaway and its influence on the East Asian monsoon: a climate model study. Geol. Soc. Lond., Spec. Publ. 342, 265–277.
Mullender, T.A.T., van Velzen, A.J., Dekkers, M.J., 1993. Continuous drift correction and separate identification of ferrimagnetic and paramagnetic contributions in thermomagnetic runs. Geophys. J. Int. 114, 663–672.
Nie, J., Peng, W., 2014. Automated SEM–EDS heavy mineral analysis reveals no provenance shift between glacial loess and interglacial paleosol on the Chinese Loess Plateau. Aeolian Res. 13, 71–75.
Nie, J., King, J.W., Fang, X., 2007. Enhancement mechanisms of magnetic susceptibility in the Chinese red-clay sequence. Geophys. Res. Lett. 34, L19705. http://dx.doi.org/10.11029/12007GL031430.
Nie, J.S., King, J., Fang, X.M., 2008a. Correlation between the magnetic susceptibility record of the Chinese aeolian sequences and the marine benthic oxygen isotope record. Geochem. Geophys. Geosyst. 9, Q12026. http://dx.doi.org/10.11029/12008GC002243.
Nie, J.S., King, J., Jackson, M., Fang, X.M., Song, Y.G., 2008b. AC magnetic susceptibility studies of Chinese red clay sediments between 4.8 and 4.1 Ma: paleoceanographic and paleoclimatic implications. J. Geophys. Res. Solid Earth 113, B10106. http://dx.doi.org/10.11029/12008JB005654.
Nie, J.S., King, J.W., Fang, X.M., 2008c. Link between benthic oxygen isotopes and magnetic susceptibility in the red-clay sequence on the Chinese Loess Plateau. Geophys. Res. Lett. 35, L03703. http://dx.doi.org/10.01029/02007gl032817.
Nie, J.S., Song, Y.G., King, J.W., Egli, R., 2010a. Consistent grain size distribution of pedogenic maghemite of surface soils and Miocene loessic soils on the Chinese Loess Plateau. J. Quat. Sci. 25, 261–266.
Nie, J.S., Song, Y.G., King, J.W., Fang, X.M., Heil, C., 2010b. HIRM variations in the Chinese red-clay sequence: insights into pedogenesis in the dust source area. J. Asian Earth Sci. 38, 96–104.
Nie, J.S., Song, Y.G., King, J.W., Zhang, R., Fang, X.M., 2013. Six million years of magnetic grain-size records reveal that temperature and precipitation were decoupled on the Chinese Loess Plateau during similar to 4.5–2.6 Ma. Quat. Res. 79, 465–470.
Nie, J.S., Peng, W.B., Moller, A., Song, Y.G., Stockli, D.F., Stevens, T., Horton, B.K., Liu, S.P., Bird, A., Oalmann, J., Gong, H.J., Fang, X.M., 2014a. Provenance of the upper Miocene-Pliocene Red Clay deposits of the Chinese Loess Plateau. Earth Planet. Sci. Lett. 407, 35–47.
Nie, J.S., Stevens, T., Song, Y.G., King, J.W., Zhang, R., Ji, S.C., Gong, L.S., Cares, D., 2014b. Pacific freshening drives Pliocene cooling and Asian monsoon intensification. Sci Rep 4, 5474. http://dx.doi.org/10.1038/srep05474.
Nie, J.S., Zhang, R., Necula, C., Heslop, D., Liu, Q.S., Gong, L.S., Banerjee, S., 2014c. Late Miocene- early Pleistocene paleoclimate history of the Chinese Loess Plateau revealed by remanence unmixing. Geophys. Res. Lett. 41, 2163–2168.
Nie, J., Stevens, T., Rittner, M., Stockli, D., Garzanti, E., Limonta, M., Bird, A., Andò, S., Vermeesch, P., Saylor, J., Lu, H., Breecker, D., Hu, X., Liu, S., Resentini, A., Vezzoli, G., Peng, W., Carter, A., Ji, S., Pan, B., 2015. Loess Plateau storage of Northeastern Tibetan Plateau-derived Yellow River sediment. Nat. Commun. 6, 8511. http://dx.doi.org/10.1038/ncomms9511.
Nie, J., Song, Y., King, J.W., 2016. A review of recent advances in red-clay environmental magnetism and paleoclimate history on the Chinese Loess Plateau. Front. Earth Sci. 4, 27. http://dx.doi.org/10.3389/feart.2016.00027.
Paillard, D., Parrenin, F., 2004. The Antarctic ice sheet and the triggering of deglaciations. Earth Planet. Sci. Lett. 227, 263–271.
Paillard, D., Labeyrie, L., Yiou, P., 1996. Analyseries 1.0: a Macintosh software for the analysis of geographical time-series. Eos 77, 379.
Peng, W.B., Wang, Z., Song, Y.G., Pfaff, K., Luo, Z., Nie, J.S., Chen, W.H., 2016. A comparison of heavy mineral assemblage between the loess and the Red Clay sequences on the Chinese Loess Plateau. Aeolian Res. 21, 87–91.
Qiang, X.K., Li, Z.X., Powell, C.M., Zheng, H.B., 2001. Magnetostratigraphic record of the Late Miocene onset of the East Asian monsoon, and Pliocene uplift of northern Tibet. Earth Planet. Sci. Lett. 187, 83–93.
Qiang, X.K., An, Z.S., Li, H.M., Chang, H., Song, Y.G., 2005. Magnetic properties of Jiaxian red clay sequences from northern Chinese Loess Plateau and its paleoclimatic significance. Sci. China Ser. D Earth Sci. 48, 1234–1245.
Qiang, X.K., An, Z.S., Song, Y.G., Chang, H., Sun, Y.B., Liu, W.G., Ao, H., Dong, J.B., Fu, C.F., Wu, F., Lu, F.Y., Cai, Y.Y., Zhou, W.J., Cao, J.J., Xu, X.W., Ai, L., 2011. New eolian red clay sequence on the western Chinese Loess Plateau linked to onset of Asian desertification about 25 Ma ago. Sci. China Earth Sci. 54, 136–144.
Ramstein, G., Fluteau, F., Besse, J., Joussaume, S., 1997. Effect of orogeny, plate motion and land-sea distribution on Eurasian climate change over the past 30 million years. Nature 386, 788–795.
Rea, D.K., Snoeckx, H., Joseph, L.H., 1998. Late Cenozoic eolian deposition in the North Pacific: Asian drying, Tibetan uplift, and cooling of the northern hemisphere. Paleoceanography 13, 215–224.
Schwertmann, U., 1971. Transformation of Hematite to Goethite in Soils. Nature 232, 624–625.
Song, Y.G., Fang, X.M., Li, J.J., An, Z.S., Miao, X.D., 2001a. The Late Cenozoic uplift of the Liupan Shan, China. Sci. China Ser. D Earth Sci. 44, 176–184.
Song, Y.G., Fang, X.M., Masayuki, T., Naoto, I., Li, J.J., An, Z.S., 2001b. Magnetostratigraphy of Late Tertiary sediments from the Chinese Loess Plateau and its paleoclimatic significance. Chin. Sci. Bull. 46, 16–22.
Song, Y.G., Fang, X.M., Dong, H.M., Qiang, X.K., Chang, H., Fu, C.F., Fu, K.D., 2005. Geochronological and stratigraphical evidences for the uplift of the Liupan Shan, Northeastern boundary of the Tibetan Plateau. In: IEEE International Geoscience and Remote Sensing Symposium. Institute of Electrical and Electronics Engineers Inc., Seoul, Korea, pp. 5223–5226.
Song, Y.G., Fang, X.M., Torii, M., Ishikawa, N., Li, J.J., An, Z.S., 2007. Late Neogene rock magnetic record of climatic variation from Chinese eolian sediments related to uplift of the Tibetan Plateau. J. Asian Earth Sci. 30, 324–332.
Song, Y., Hao, Q., Ge, J., Zhao, D.a., Zhang, Y., Li, Q., Zuo, X., Lü, Y., Wang, P., 2014. Quantitative relationships between magnetic enhancement of modern soils and climatic variables over the Chinese Loess Plateau. Quat. Int. 334, 119–131.
Song, Y.G., Fang, X.M., King, J.W., Li, J.J., Naoto, I., An, Z.S., 2014. Magnetic parameter variations in the Chaona loess/paleosol sequences in the central Chinese Loess Plateau, and their significance for the middle Pleistocene climate transition. Quat. Res. 81, 433–444.
Steinke, S., Groeneveld, J., Johnstone, H., Rendle-Buhring, R., 2010. East Asian summer monsoon weakening after 7.5 Ma: evidence from combined planktonic foraminifera Mg/Ca and delta O-18 (ODP Site 1146; northern South China Sea). Palaeogeogr. Palaeoclimatol. Palaeoecol. 289, 33–43.
Sun, Y.B., An, Z.S., 2002. History and variability of Asian interior aridity recorded by eolian flux in the Chinese Loess Plateau during the past 7 Ma. Sci. China Ser. D Earth Sci. 45, 420–429.
Sun, X., Wang, P., 2005. How old is the Asian monsoon system?–palaeobotanical records from China. Palaeogeogr. Palaeoclimatol. Palaeoecol. 222, 181–222.
Sun, D.H., An, Z.S., Shaw, J., Bloemendal, J., Sun, Y.B., 1998a. Magnetostratigraphy and paleoclimatic significance of Late Tertiary aeolian sequences in the Chinese Loess Plateau. Geophys. J. Int. 134, 207–212.
Sun, D.H., Shaw, J., An, Z.S., Cheng, M.Y., Yue, L.P., 1998b. Magnetostratigraphy and paleoclimatic interpretation of a continuous 7.2 Ma Late Cenozoic Eolian sediments from the Chinese Loess Plateau. Geophys. Res. Lett. 25, 85–88.
Sun, Y.B., Lu, H.Y., An, Z.S., 2006. Grain size of loess, palaeosol and Red Clay deposits on the Chinese Loess Plateau: significance for understanding pedogenic alteration and palaeomonsoon evolution. Palaeogeogr. Palaeoclimatol. Palaeoecol. 241, 129–138.
Sun, Y., An, Z., Clemens, S.C., Bloemendal, J., Vandenberghe, J., 2010. Seven million years of wind and precipitation variability on the Chinese Loess Plateau. Earth Planet.

Sci. Lett. 297, 525–535.
Sun, Y.B., Clemens, S.C., Morrill, C., Lin, X.P., Wang, X.L., An, Z.S., 2012. Influence of Atlantic meridional overturning circulation on the East Asian winter monsoon. Nat. Geosci. 5, 46–49.
Thompson, R., Oldfield, F., 1986. Environmental Magnetism. Allen & Unwin, London.
Torii, M., Fukuma, K., Horng, C.S., Lee, T.Q., 1996. Magnetic discrimination of pyrrhotite- and greigite-bearing sediment samples. Geophys. Res. Lett. 23, 1813–1816.
Vandenberghe, J., Lu, H.Y., Sun, D.H., van Huissteden, J., Konert, M., 2004. The late Miocene and Pliocene climate in East Asia as recorded by grain size and magnetic susceptibility of the Red Clay deposits (Chinese Loess Plateau). Palaeogeogr. Palaeoclimatol. Palaeoecol. 204, 239–255.
VanVelzen, A.J., Dekkers, M.J., 1999. The incorporation of thermal methods in mineral magnetism of loess-paleosol sequences: a brief overview. Chin. Sci. Bull. 44, 53–63.
Wan, S.M., Li, A.C., Clift, P.D., Jiang, H.Y., 2006. Development of the East Asian summer monsoon: evidence from the sediment record in the South China Sea since 8.5 Ma. Palaeogeogr. Palaeoclimatol. Palaeoecol. 241, 139–159.
Wang, Y.-X., Yang, J.-D., Chen, J., Zhang, K.-J., Rao, W.-B., 2007. The Sr and Nd isotopic variations of the Chinese Loess Plateau during the past 7 Ma: implications for the East Asian winter monsoon and source areas of loess. Palaeogeogr. Palaeoclimatol. Palaeoecol. 249, 351–361.
Wu, F.L., Fang, X.M., Ma, Y.Z., Herrmann, M., Mosbrugger, V., An, Z.S., Miao, Y.F., 2007. Plio–quaternary stepwise drying of Asia: evidence from a 3-Ma pollen record from the Chinese Loess Plateau. Earth Planet. Sci. Lett. 257, 160–169.
Xu, Y., Yue, L., Li, J., Sun, L., Sun, B., Zhang, J., Ma, J., Wang, J., 2009. An 11-Ma-old red clay sequence on the Eastern Chinese Loess Plateau. Palaeogeogr. Palaeoclimatol. Palaeoecol. 284, 383–391.
Yue, L., Heller, F., Qiu, Z., Zhang, L., Xie, G., Qiu, Z., Zhang, Y., 2001. Magnetostratigraphy and pavleo-environmental record of Tertiary deposits of Lanzhou Basin. Chin. Sci. Bull. 46, 770–773.
Yue, L., Li, J., Zheng, G., Li, Z., 2007. Evolution of the Ordos Plateau and environmental effects. Sci. China Ser. D Earth Sci. 50, 19–26.
Zachos, J.C., Dickens, G.R., Zeebe, R.E., 2008. An early Cenozoic perspective on greenhouse warming and carbon-cycle dynamics. Nature 451, 279–283.
Zan, J., Fang, X., Yan, M., Li, B., 2017. New insights into the palaeoclimatic interpretation of the temperature dependence of the magnetic susceptibility and magnetization of Mid-Late Pleistocene loess/palaeosols in Central Asia and the Chinese Loess Plateau. Geophys. J. Int. 208, 663–673.
Zhang, Z., Wang, H., Guo, Z., Jiang, D., 2007. What triggers the transition of palaeoenvironmental patterns in China, the Tibetan Plateau uplift or the Paratethys Sea retreat? Palaeogeogr. Palaeoclimatol. Palaeoecol. 245, 317–331.
Zhang, R., Necula, C., Heslop, D., Nie, J., 2016. Unmixing hysteresis loops of the late Miocene–early Pleistocene loess-red clay sequence. Sci Rep 6, e29515. http://dx.doi.org/10.21038/srep29515.
Zhou, L.P., Oldfield, F., Wintle, A.G., Robinson, S.G., Wang, J.T., 1990. Partly pedogenic origin of magnetic variations in Chinese loess. Nature 346, 737–739.
Zhu, R.X., Pan, Y.X., Ding, Z.L., 1996. Magnetic property of red clay. J. Quat. Sci. 16, 232–238 (In Chinese with English abstract).
Zhu, Y., Zhou, L., Mo, D., Kaakinen, A., Zhang, Z., Fortelius, M., 2008. A new magnetostratigraphic framework for late Neogene Hipparion Red Clay in the eastern Loess Plateau of China. Palaeogeogr. Palaeoclimatol. Palaeoecol. 268, 47–57.